ARMY RESEARCH LABORATORY

Experimental Evaluation of Dynamic Crack Branching in Poly(methyl methacrylate) (PMMA) Using the Method of Coherent Gradient Sensing

by Pierce Umberger

ARL-CR-637 **February 2010**

prepared by

Oak Ridge Institute for Science and Education
4692 Millennium Dr., Ste. 101
Belcamp, MD 21017

under contract

ORISE-1120-1120-99

NOTICES

Disclaimers

The findings in this report are not to be construed as an official Department of the Army position unless so designated by other authorized documents.

Citation of manufacturer's or trade names does not constitute an official endorsement or approval of the use thereof.

Destroy this report when it is no longer needed. Do not return it to the originator.

Army Research Laboratory
Aberdeen Proving Ground, MD 21005-5066

ARL-CR-637 **February 2010**

Experimental Evaluation of Dynamic Crack Branching in Poly(methyl methacrylate) (PMMA) Using the Method of Coherent Gradient Sensing

Pierce Umberger

prepared by

Oak Ridge Institute for Science and Education
4692 Millennium Dr., Ste. 101
Belcamp, MD 21017

under contract

ORISE-1120-1120-99

REPORT DOCUMENTATION PAGE	Form Approved OMB No. 0704-0188

1. REPORT DATE *(DD-MM-YYYY)*	2. REPORT TYPE	3. DATES COVERED (From - To)
February 2010	Final	Summer 2009

4. TITLE AND SUBTITLE
Experimental Evaluation of Dynamic Crack Branching in Poly(methyl methacrylate) (PMMA) Using the Method of Coherent Gradient Sensing

5a. CONTRACT NUMBER
ORISE-1120-1120-99

5b. GRANT NUMBER

5c. PROGRAM ELEMENT NUMBER

6. AUTHOR(S)
Pierce Umberger

5d. PROJECT NUMBER

5e. TASK NUMBER

5f. WORK UNIT NUMBER

7. PERFORMING ORGANIZATION NAME(S) AND ADDRESS(ES)
Oak Ridge Institute for Science and Education
4692 Millennium Dr., Ste. 101
Belcamp, MD 21017

8. PERFORMING ORGANIZATION REPORT NUMBER

9. SPONSORING/MONITORING AGENCY NAME(S) AND ADDRESS(ES)
U.S. Army Research Laboratory
RDRL-WMP-D
Aberdeen Proving Ground, MD 21005-5066

10. SPONSOR/MONITOR'S ACRONYM(S)
ARL

11. SPONSOR/MONITOR'S REPORT NUMBER(S)
ARL-CR-637

12. DISTRIBUTION/AVAILABILITY STATEMENT
Approved for public release; distribution is unlimited.

13. SUPPLEMENTARY NOTES

14. ABSTRACT
We investigate the experimental setup and methods to evaluate the characteristics of dynamic crack branching in poly(methyl methacrylate) (PMMA). The method of coherent gradient sensing is used to determine crack tip location and crack mode mixity in samples dynamically loaded via a projectile from a gas gun. We study crack propagation velocities as a function of impact velocity and its effect on crack path and branching. We also note the effect of branching on crack velocity as one or more cracks move through a material.

15. SUBJECT TERMS
dynamic fracture, coherent gradient sensing, PMMA

16. SECURITY CLASSIFICATION OF:			17. LIMITATION OF ABSTRACT	18. NUMBER OF PAGES	19a. NAME OF RESPONSIBLE PERSON
a. REPORT	b. ABSTRACT	c. THIS PAGE			Bryan Love
Unclassified	Unclassified	Unclassified	UU	76	19b. TELEPHONE NUMBER (*Include area code*) 410-278-3707

Standard Form 298 (Rev. 8/98)
Prescribed by ANSI Std. Z39.18

Contents

List of Figures

List of Tables

Acknowledgments

Gracious thanks are extended to Dr. Bryan Love, U.S. Army Research Laboratory (ARL), for providing extensive academic and technical support throughout the duration of this work and to Mr. William Edmanson for his constant help in lab setup, sample preparation, and test execution. Additional thanks to the other ARL personnel too numerous to list who provided assistance throughout the course of this research.

This research was supported in part by an appointment to the Student Research Participation program at ARL administered by the Oak Ridge Institute for Science and Education through an interagency agreement between the U.S. Department of Energy and ARL.

1. Introduction

The problem of single or multiple cracks propagating in a solid has been studied for some time. In 1951, Yoffe (*1*) developed a simplified theoretical solution for a crack of constant length moving uniformly through a solid. As the crack tip travels across the solid, the back closes, maintaining the constant crack length. This method reduced the problem because there is no energy radiated away from the crack itself, simplifying the energy balance. Yoffe predicted the Rayleigh wave speed as the maximum crack speed in the solid. In 1959, Schardin (*2*) observed crack branching occurring at speeds significantly lower than (<70%) the Rayleigh wave speed predicted by Yoffe's simplified analytical solution in inorganic glasses using the multiple spark camera technique.

In addition to Schardin's multiple spark camera technique, there have been several methods of measuring crack speed. Wallner (*3*) observed that interactions between the crack and shear waves resulting from the fracture produced undulations on the crack surface and hypothesized that these undulations—Wallner lines—could be used to determine crack speed postmortem. Kerkhof (*4*) used ultrasonic transducers to generate stress waves that left regular undulation patters on the fracture surface, allowing crack speed to be measured postmortem.

Ravi-Chandar and Knauss (*5*), as well as Kalthoff (*6*, *7*) and others, investigated the behavior of cracks, including branching phenomena, under dynamic loading using high-speed photography and again observed that branching occurred well below the Rayleigh wave speed. Building on Schardin's multiple spark camera technique (*2*), Theocaris (*8*) used a reflected shadow method to study cracked plates. Rosakis and Ravi-Chandar (*9*) used a refined method of caustics to evaluate three-dimensional effects in crack formation.

In 1991, Tippur et al. (*10*) developed coherent gradient sensing (CGS) in reflection to measure material deformations close to a crack tip. They later extended this method to transmission as well (*11*). CGS is a lateral-shearing interferometric method that uses a beam of collimated, coherent light either passed through or reflected off a specimen. The light is then directed through a pair of identical diffraction gratings and a filtering lens. A series of diffraction orders is produced, and the +1 or –1 order is viewed on a focal plane with a filtering aperture. A resulting light/dark fringe pattern represents the out-of-plane displacement gradients with respect to the principal direction of the gratings.

There have been many studies in cracks propagating in poly(methyl methacrylate) (PMMA). Sharon et al. (*12*) investigated the presence of microscopic local attempted crack branching as a possible source for instability in dynamic fracture. Broberg (*13*) used PMMA to study crack paths under dynamic loading, particularly localized mode I fracture in cases of global mode II or

III loading. He also discusses crack branching as it relates to preferential mode I fracture. Bjerke and Lambros (*14*) studied thermomechanical effects at the tip of propagating cracks in PMMA, in particular, the relation to crack speed.

In 1990, Freund published Dynamic Fracture Mechanics (*15*), a summary of the history and state of the art of the dynamic fracture field, including experimental methods and results. It provides an excellent overview of the field as well as detailed accounts of solutions to many dynamic fracture problems.

2. Experimental Evaluation

2.1 Test Setup

2.1.1 Sample and Projectile Geometry

Approximately 75 borosilicate glass and 100 PMMA samples were produced for testing. Glass samples were nominally 6 and 12 mm thick, and PMMA samples were nominally 13 mm thick. Sample dimensions are shown in figure 1.

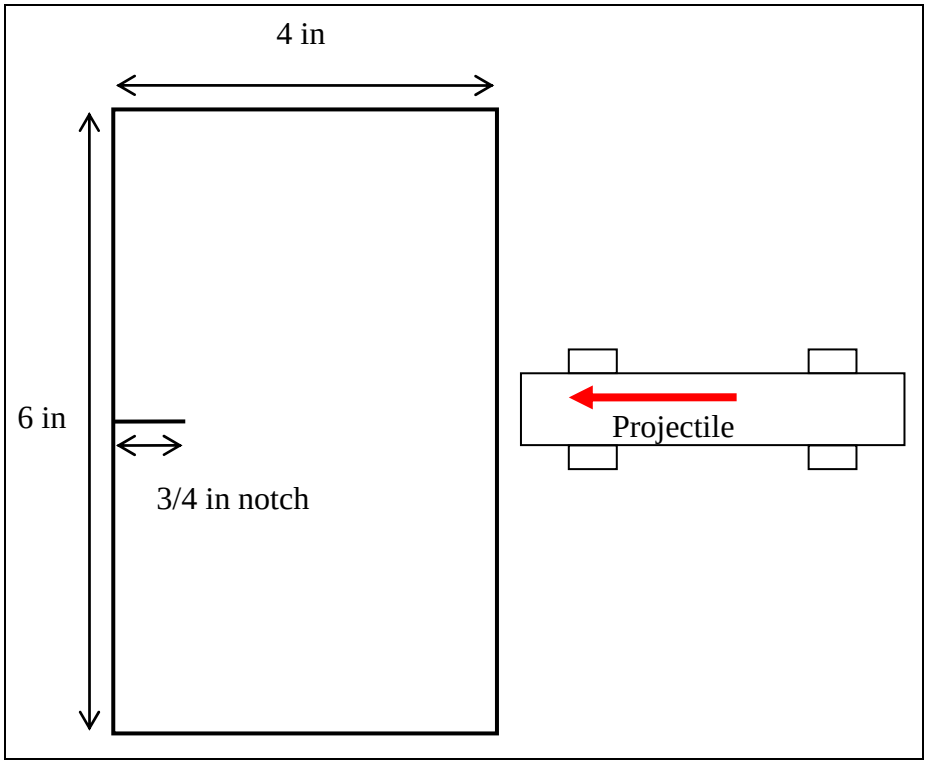

Figure 1. Mode I test sample geometry. Samples were 6, 12, or 13 mm thick.

All testing was conducted at the U.S. Army Research Laboratory at Aberdeen Proving Ground, MD. A 67-g cylindrical aluminum projectile was fired at the target to induce a mode I opening crack at the tip of a premachined notch. The crack was observed as it traversed the specimen from left to right.

2.1.2 Gas Gun Setup

Projectiles were launched at the target using a single-stage light gas gun at pressures ranging from 34 to 345 kPa (5 to 50 psi), achieving projectile velocities of ~20–70 m/s. Figures 2 and 3 show the gas gun and projectile, respectively.

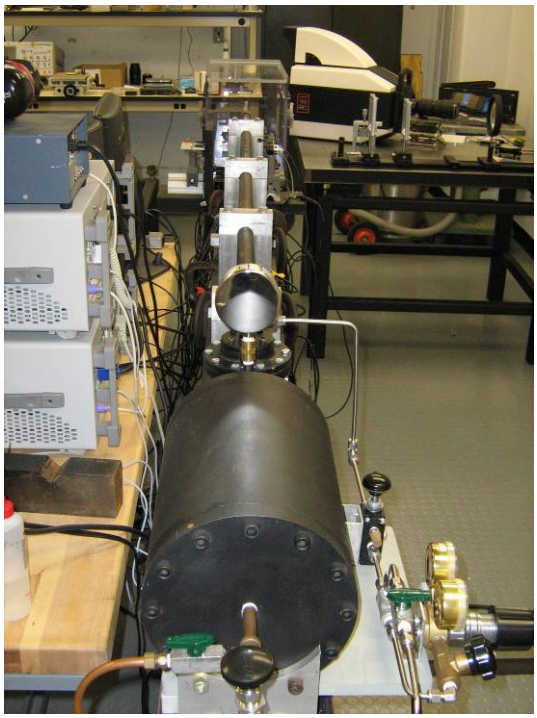

Figure 2. Gas gun setup. The specimen is mounted in a polycarbonate box at the top of the picture.

Figure 3. Aluminum projectile. Dimensions are 80 mm long × 19-mm diameter.

Specimens are mounted in a target chamber at the muzzle end of the barrel. Upon impact, data acquisition is initiated by the mechanical closing of an electrical make-screen circuit attached to the impact face of the sample, shown alone in figure 4 and installed in the target chamber in figure 5. Targets were tested in two basic configurations—sitting unconstrained and backed by a support to induce three-point bending on impact. Additionally, two lasers were directed through ports perpendicular to the gun barrel, with the beam intensity monitored by phototransistors. The time delay between the projectile breaking the two laser beams provided velocity information. These sensors can be seen in figure 6 on the right side.

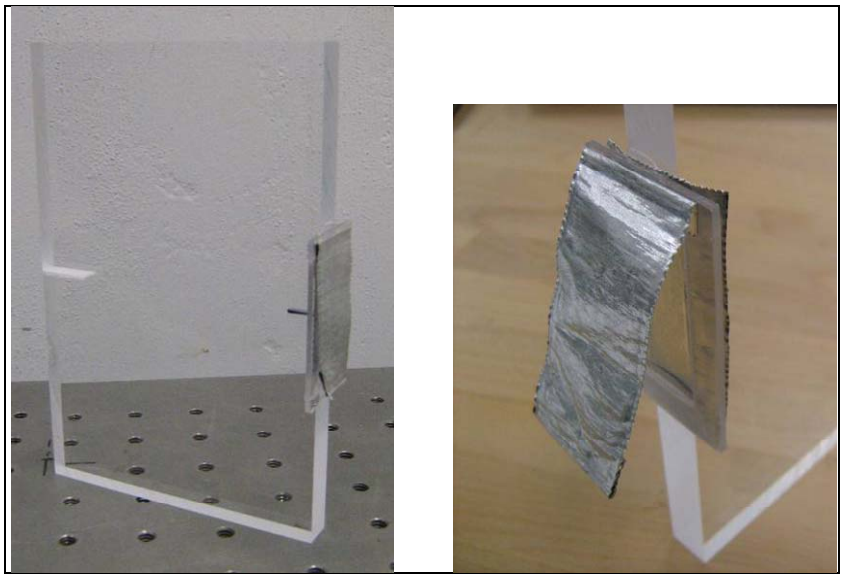

Figure 4. Prepared sample. Impact creates electrical continuity on the make-screen, triggering data acquisition.

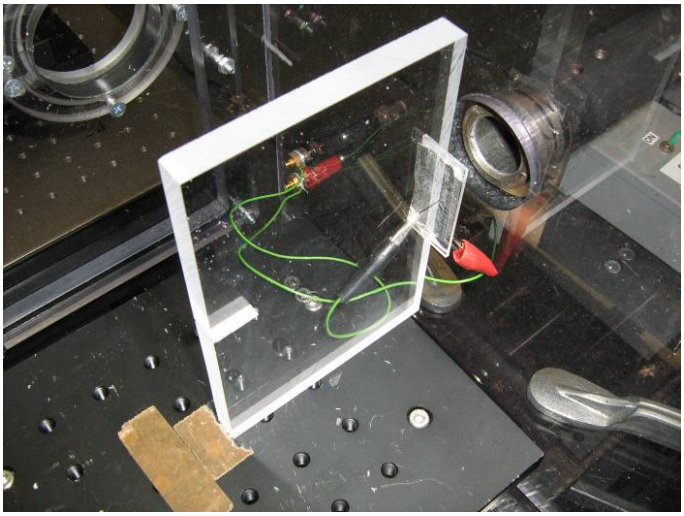

Figure 5. Sample shown in target chamber in test configuration.

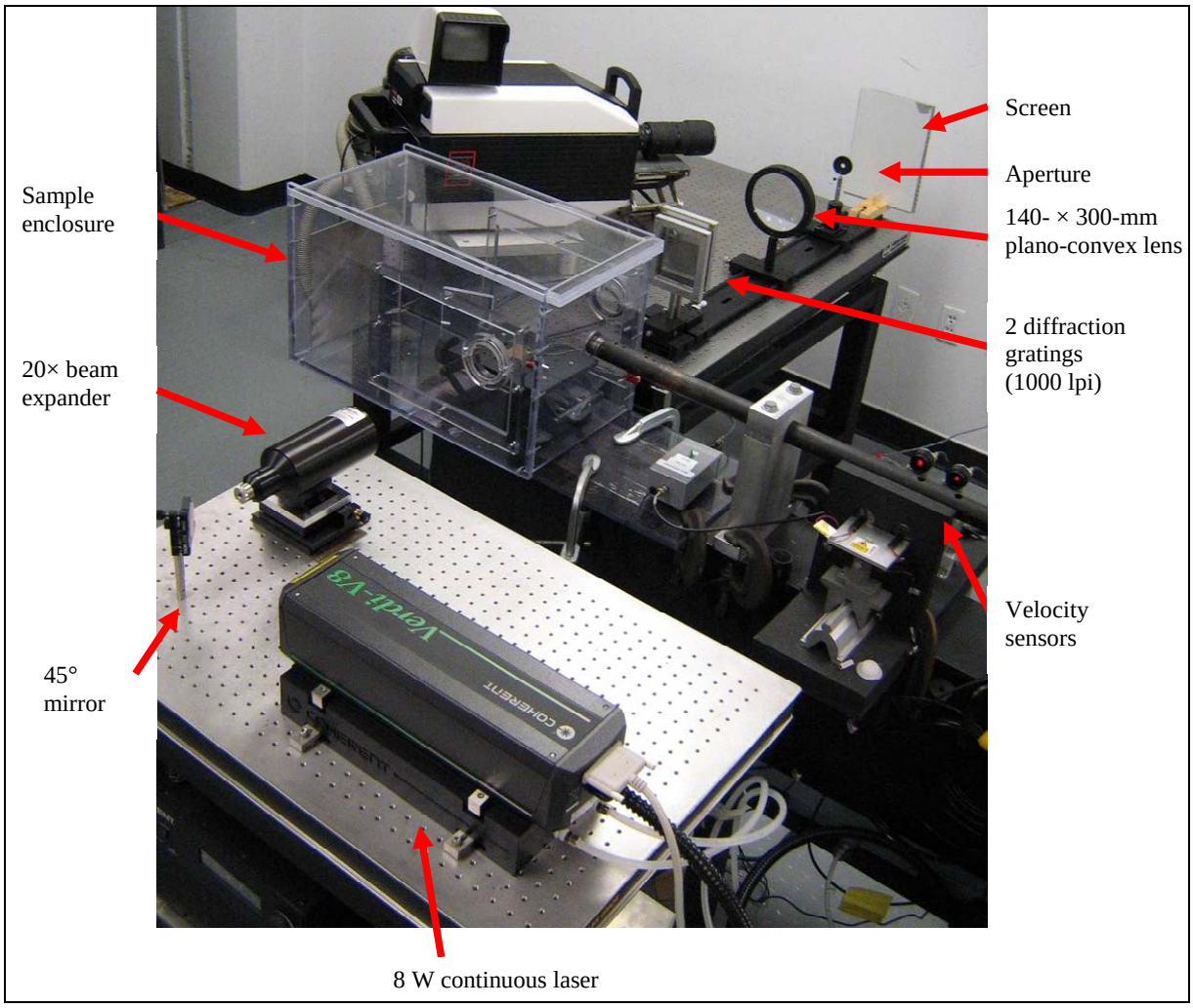

Figure 6. Major components of test setup. Optical tables on left and right side of sample chamber are aligned and parallel.

2.1.3 Laser and Optics

Crack tip location and mode mixity were determined using the method of Coherent Gradient Sensing (CGS). An 8-W, diode-pumped, solid-state (DPSS) Coherent Verdi V8 532-nm laser was expanded to a ~60 mm beam and directed through the sample, a pair of diffraction gratings, and a plano-convex lens that projected an image through an aperture onto a screen. This projected image was photographed at between 200,000 and 750,000 frames per second using a Hadland Imacon 200 high-speed camera. The test setup is shown in figure 6.

2.2 Test Sample Materials

2.2.1 Glass

Borosilicate glass was the first test material. Samples were waterjet cut (including the crack starter notch) and unpolished. The tests were first filmed directly by pointing the camera directly at the sample chamber and using a flashbulb (instead of the laser) for illumination. Figure 7 shows four frames of a 12-mm glass sample being impacted at 11 m/s.

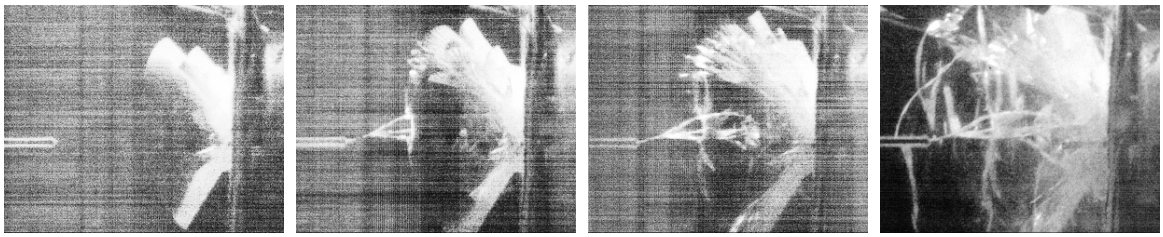

Figure 7. A 12-mm glass impact at 11 m/s. Impact is on right side of image. Note both cone crack formation at impact site and crack propagation from starter notch on left side of sample.

The major difficulty in performing this study on glass is derived from its extremely brittle nature. It was discovered that CGS did not work in glass because there was insufficient deformation at the crack tip to generate fringes. To achieve the sensitivity necessary to even begin to observe fringe patterns in glass, footsteps and work performed around the optical tables were sufficient to cause misalignment of the setup. As a result, the decision was made to switch to PMMA to test the CGS technique, allowing better identification of the crack tip location and determination of crack mode mixity.

2.2.2 PMMA

Compared to glass, PMMA exhibits relatively large deformations at the crack tip prior to failure and, thus, is a much better candidate for CGS. It was actually necessary to move the diffraction gratings closer together and decrease the fringe frequency to be able to easily distinguish the fringe patterns. There were concerns that PMMA would not be optically flat enough and would produce fringe patterns in its undeformed state; however, no such problems were observed. All results presented henceforth are for PMMA.

2.3 Fracture Response

PMMA samples were impacted at increasing velocities until the onset of crack branching. CGS images confirmed that the cracking observed is indeed mode I—fringe patterns are symmetric about the axis of crack propagation, as shown in figure 8.

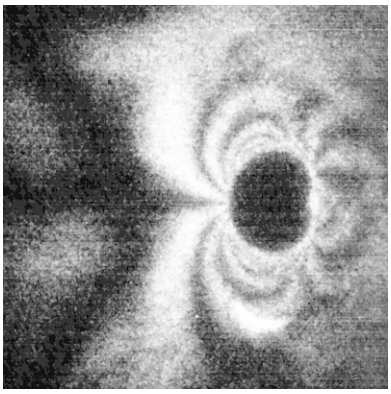

Figure 8. Fringe pattern for a crack propagation from right to left. Fringes are symmetric about the axis of crack propagation, indicating a mode I crack.

As impact velocity was increased, a slight increase in crack speed was observed. This continued until the onset of crack branching (bifurcation), at which point crack speed prior to branching appeared to reach a plateau. Figure 9 shows crack speed vs. impact velocity for PMMA samples tested.

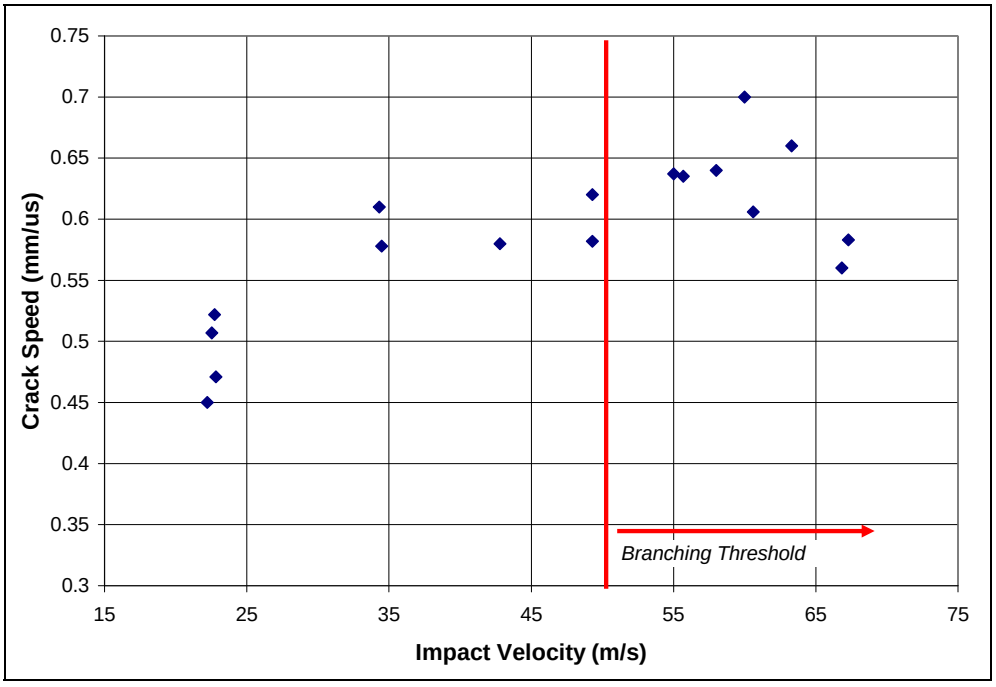

Figure 9. Crack speed vs. impact velocity. Red line indicates the impact velocity above which branching occurs regularly.

There was a distinct threshold of impact velocity above which crack branching occurred. At velocities above ~50 m/s, crack branching consistently occurred with our 67-g impactor. Figure 10 shows five frames of a crack branching from an impact velocity of ~60 m/s.

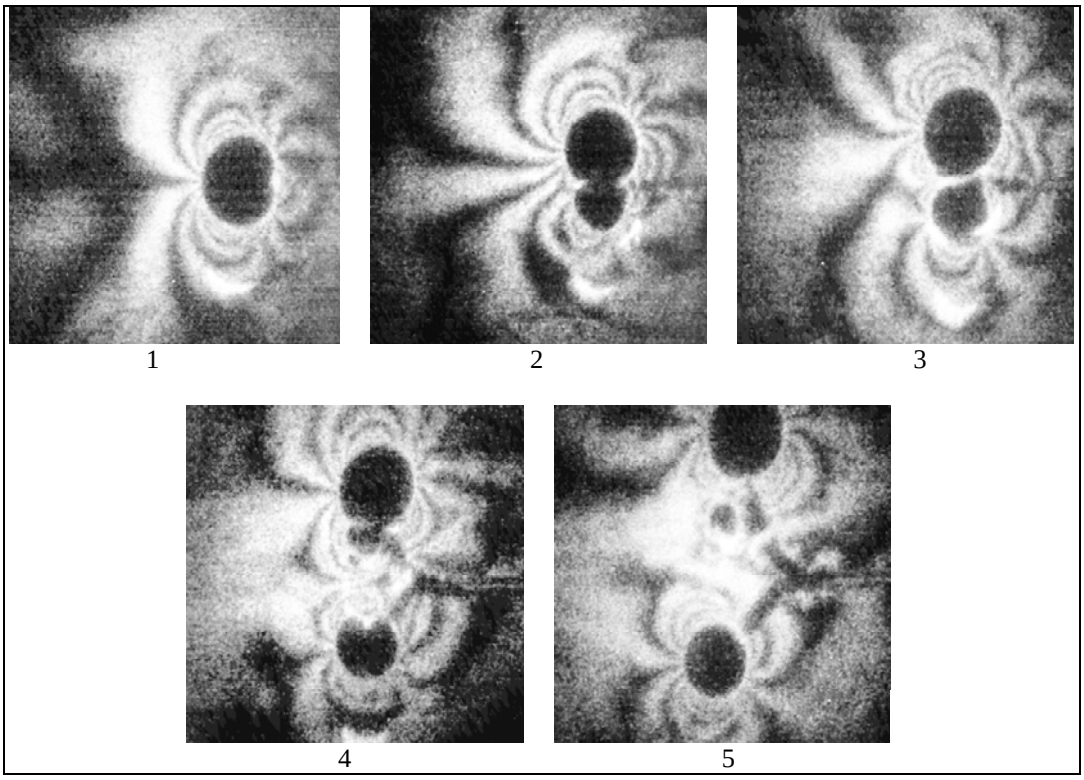

Figure 10. Crack branch formation in PMMA. Impact velocity was 60 m/s. Crack branching consistently occurs at impact velocities above 50 m/s.

The speed of a crack as it traveled through the sample was also predictable. Cracks very quickly accelerated to a constant speed and remained at that speed unless they bifurcated or self-arrested. Figure 11 shows data from two tests, both at impact velocities of 35 m/s. One sample carried a single crack all the way across, while the other branched into multiple cracks. The figure shows that both cracks initially reach the same velocity and remain relatively constant. When one crack branches, however, the velocity decreases rapidly.

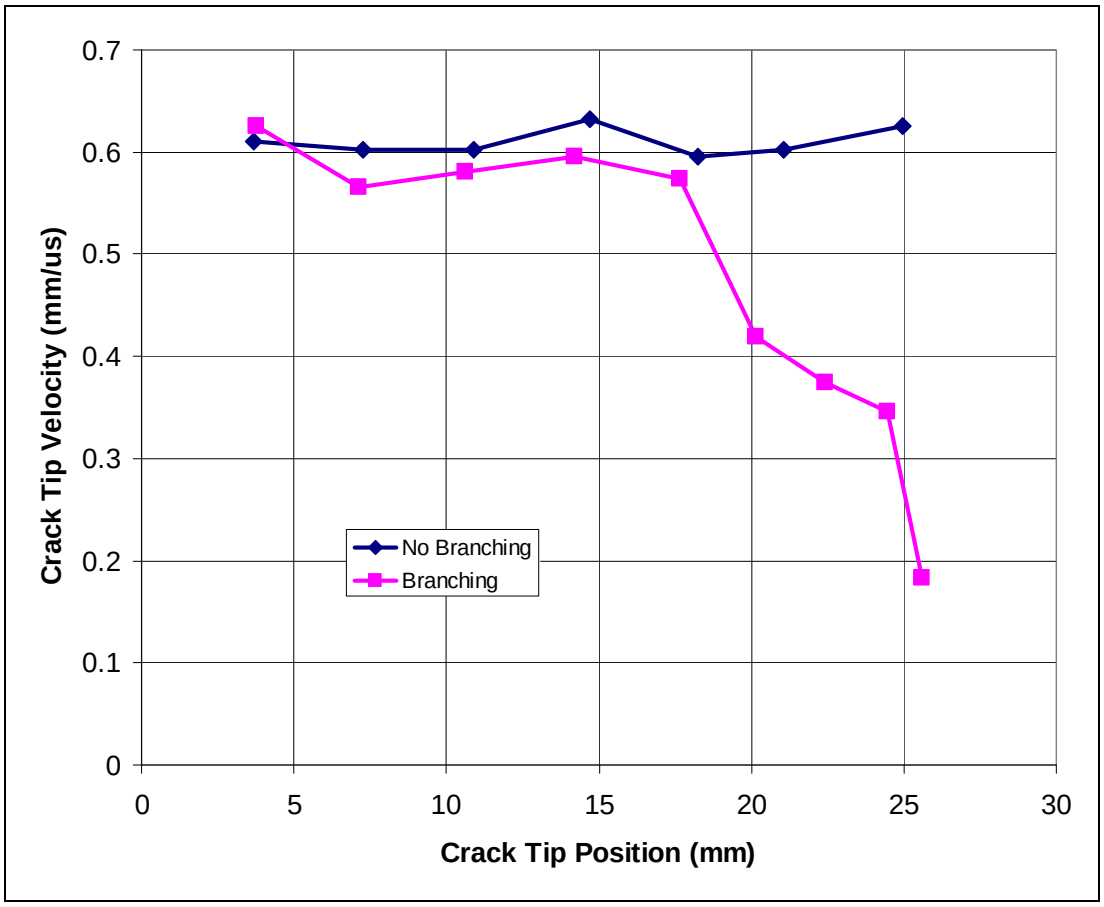

Figure 11. Crack speed vs. position in PMMA for two tests with the same impact velocity of 35 m/s.

3. Conclusions and Future Research

Driving nearly pure mode I cracks at varying velocities and inducing branching were successful. As expected, crack velocity increases with impact velocity until the onset of branching, at which point, velocity drops rapidly. Crack velocity in the sample is relatively constant on the time scale of the camera frame spacing of ~5 μs.

Since CGS did not work well with the small deformation gradients generated in glass samples, a similar study will be conducted with glass by using instead the method of caustics to identify the crack tip location and estimate the mode mixity.

4. References

1. Yoffe, E. H. The Moving Griffith Crack. *Philosophical Magazine* **1951**, *42*, 739–750.
2. Schardin, H. Velocity Effects in Fracture. In *Fracture*; Averbach, B. L., Felbeck, D. K., Hahn, G. T., Thomas, D. A., Eds.; John Wiley & Sons: New York, 1959; pp 297–329.
3. Wallner, H. Linienstrukturen an bruchflächen. *Z. Physik* **1938** *114*, 368–370.
4. Kerkhof, F. Wave Fractographic Investigation of Brittle Fracture Dynamics. In *Proceedings of the International Conference on Dynamic Crack Propagation*; Sih, G. C., Ed.; Noordhoff International Publishing: Leyden, The Netherlands, 1973; pp 3–35.
5. Ravi-Chandar, K.; Knauss, W. G. An Experimental Investigation Into Dynamic Fracture – III: Steady State Crack Propagation and Crack Branching. *Int. J. Fracture* **1984**, *26*, 141–154.
6. Kalthoff, J. F. Fracture Behavior Under High Rates of Loading. *Eng. Fract. Mech.* **1986**, *23*, 289–298.
7. Kalthoff, J. F. Transition in the Failure Behavior of Dynamically Shear Loaded Cracks. *Appl. Mech. Rev.* **1990**, *43*, 247–250.
8. Theocaris, P. S. Reflected Shadow Method for Study of Constrained Zones in Cracked Plates. *Appl. Optics* **1971**, *10*, 2240–2247.
9. Rosakis, A. J.; Ravi-Chandar, K. On Crack-Tip Stress State: An Experimental Evaluation of Three-Dimensional Effects. *Int. J. Solids Struct.* **1986**, *22*, 121–134.
10. Tippur, H. V.; Krishnaswamy, S.; Rosakis, A. J. A Coherent Gradient Sensor for Crack Tip Deformation Measurements – Analysis and Experimental Results. *Int. J. Fracture* **1991**, *48*, 193–204.
11. Tippur, H. V.; Krishnaswamy, S.; Rosakis, A. J. Optical Mapping of Crack Tip Deformations Using the Methods of Transmission and Reflection Coherent Gradient Sensing: A Study of Crack Tip K-Dominance. *Int. J. Fracture* **1991**, *52*, 91–117.
12. Sharon, E.; Gross, S. P.; Fineberg, J. Local Crack Branching as a Mechanism for Instability in Dynamic Fracture. *Phys. Rev. Lett.* **1995**, *74*, 5096–5099.
13. Broberg, K. B. On Crack Paths. *Eng. Fract. Mech.* **1987**, *28*, 663–679.
14. Bjerke, T.; Lambros, J. Heating During Shearing and Opening Dominated Dynamic Fracture of Polymers. *Exp. Mech.* **2002**, *42*, 107–114.
15. Fruend, L. B. *Dynamic Fracture Mechanics*; Cambridge University Press: Cambridge, NY, 1990.

Appendix A. Test Setup

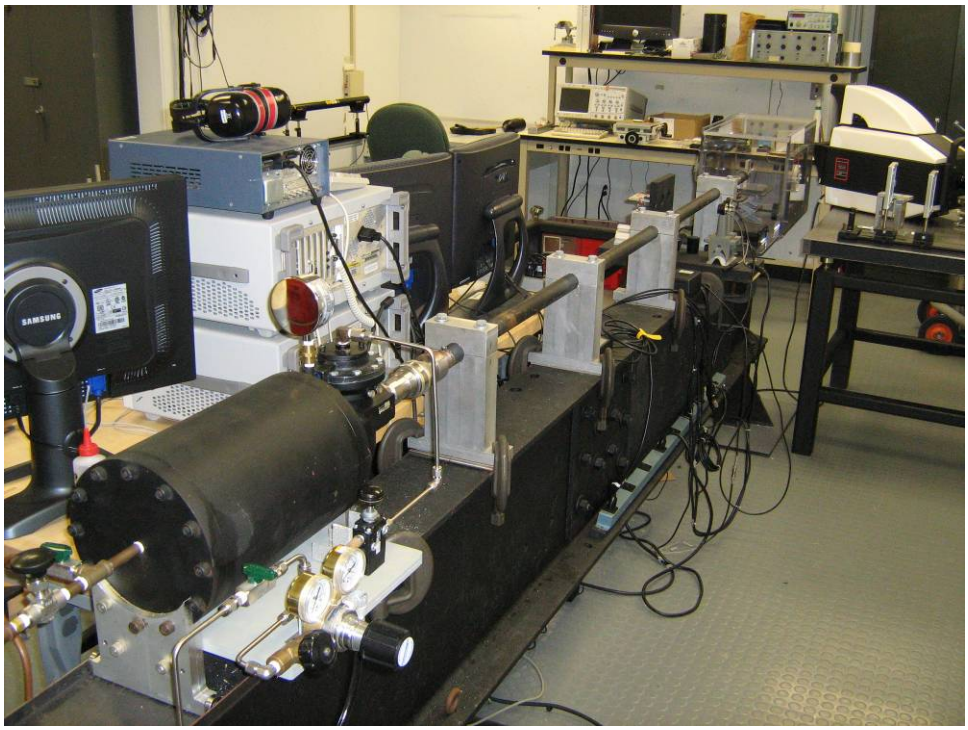

Figure A-1. Gas gun assembly.

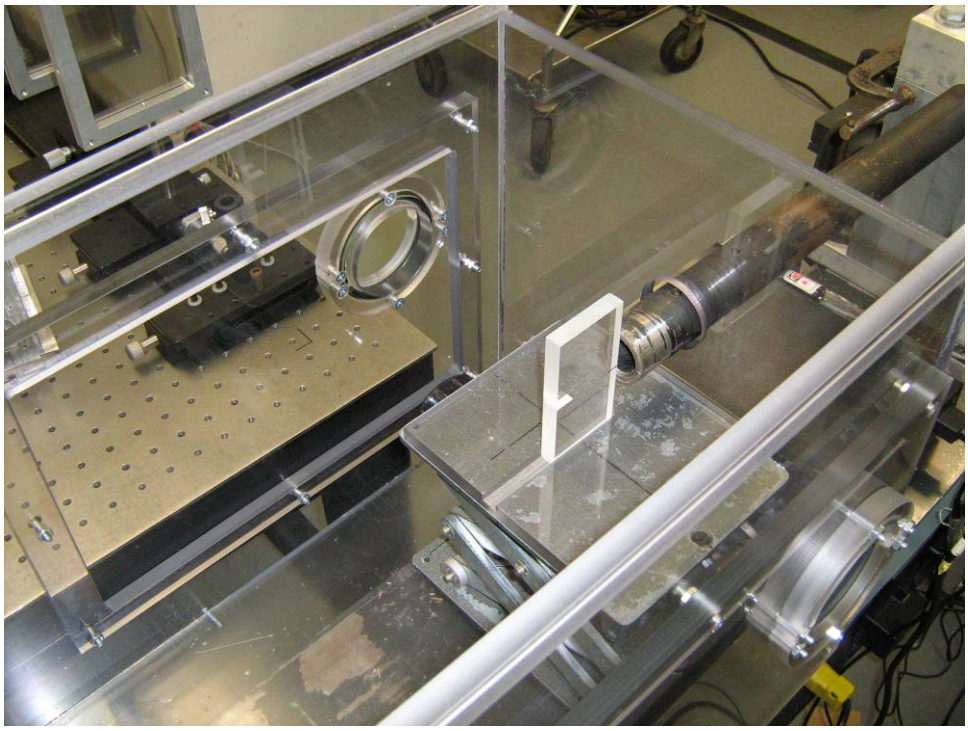

Figure A-2. Sample chamber showing test sample alignment.

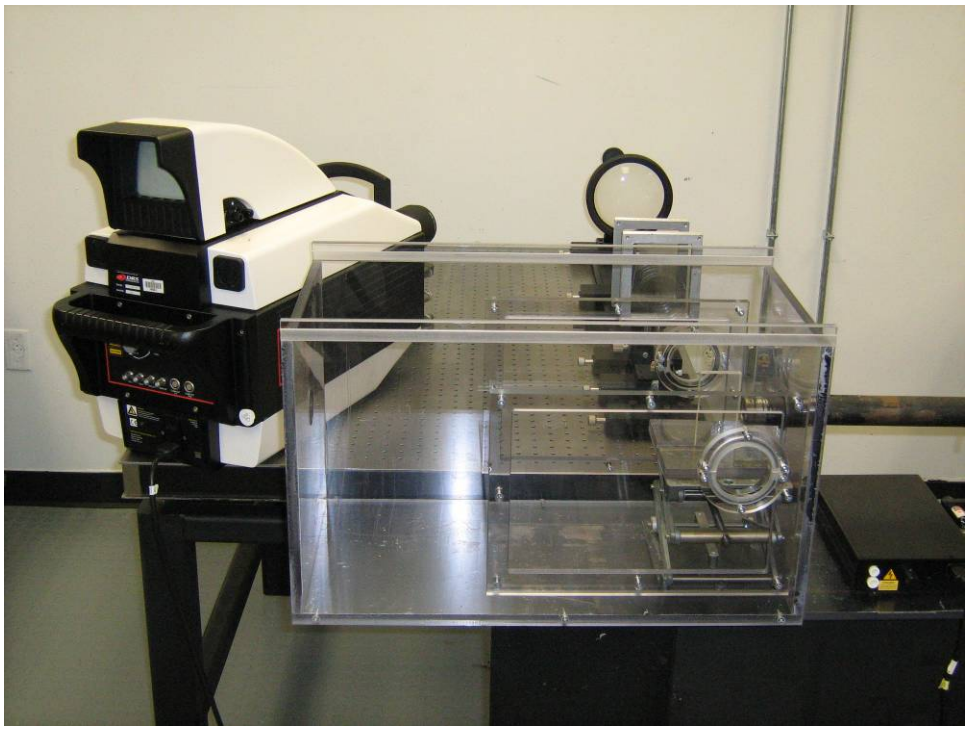

Figure A-3. Sample chamber, optics, and camera setup.

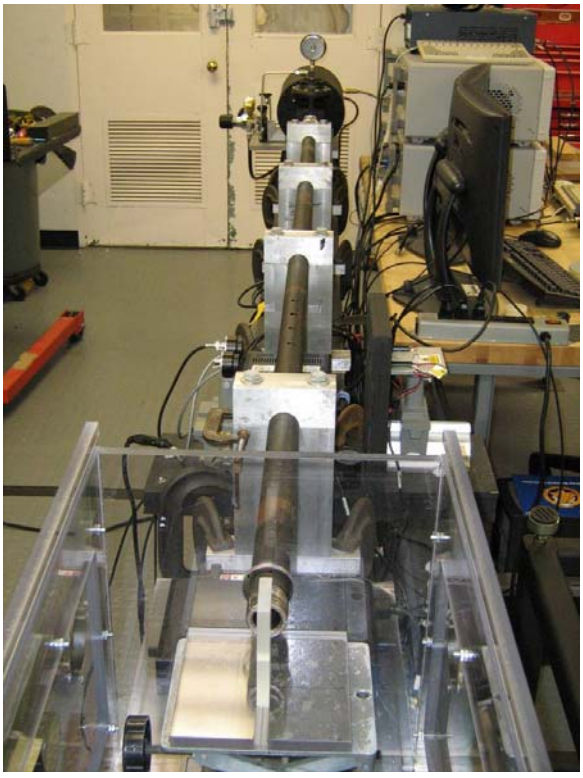

Figure A-4. Gas gun and sample chamber assembly.

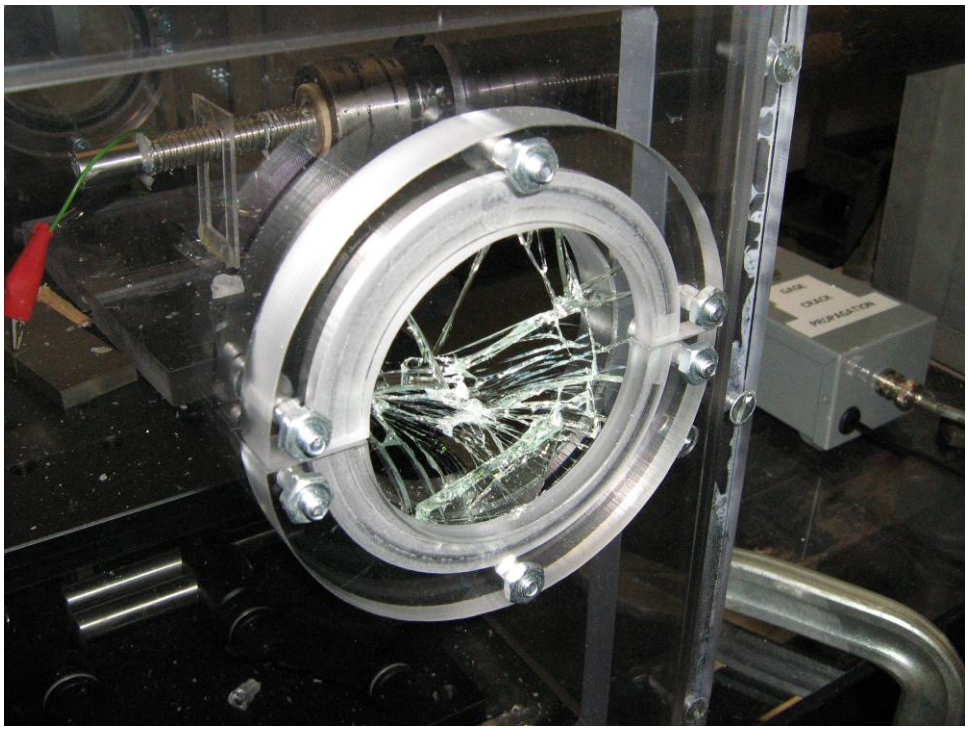

Figure A-5. Laser window cracked from stray debris during impact.

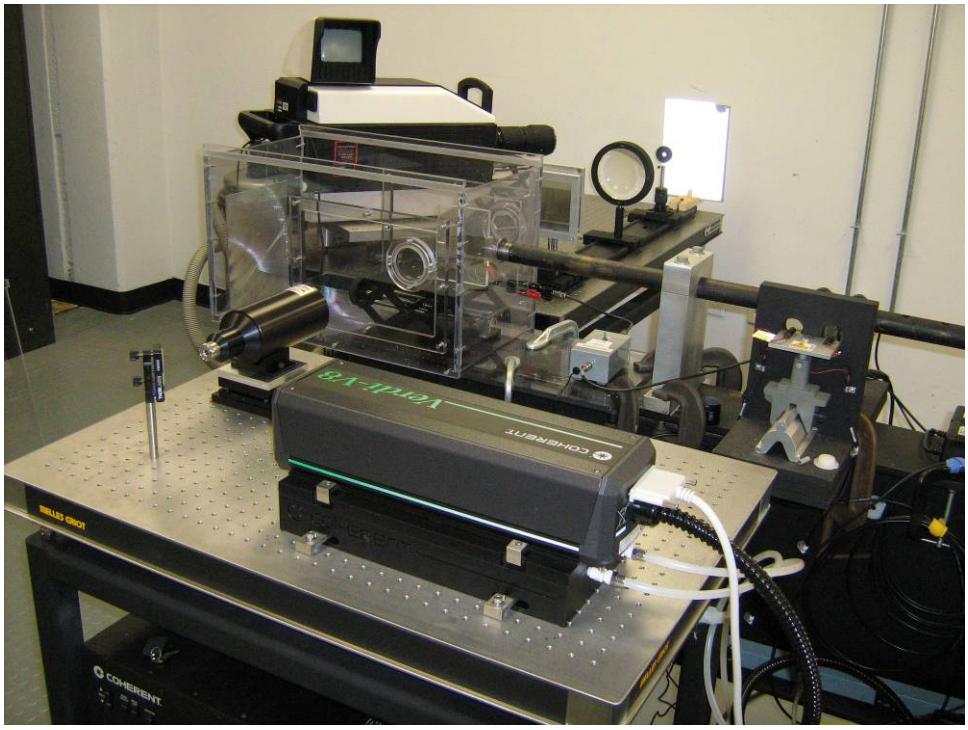

Figure A-6. Laser, optics, and test chamber.

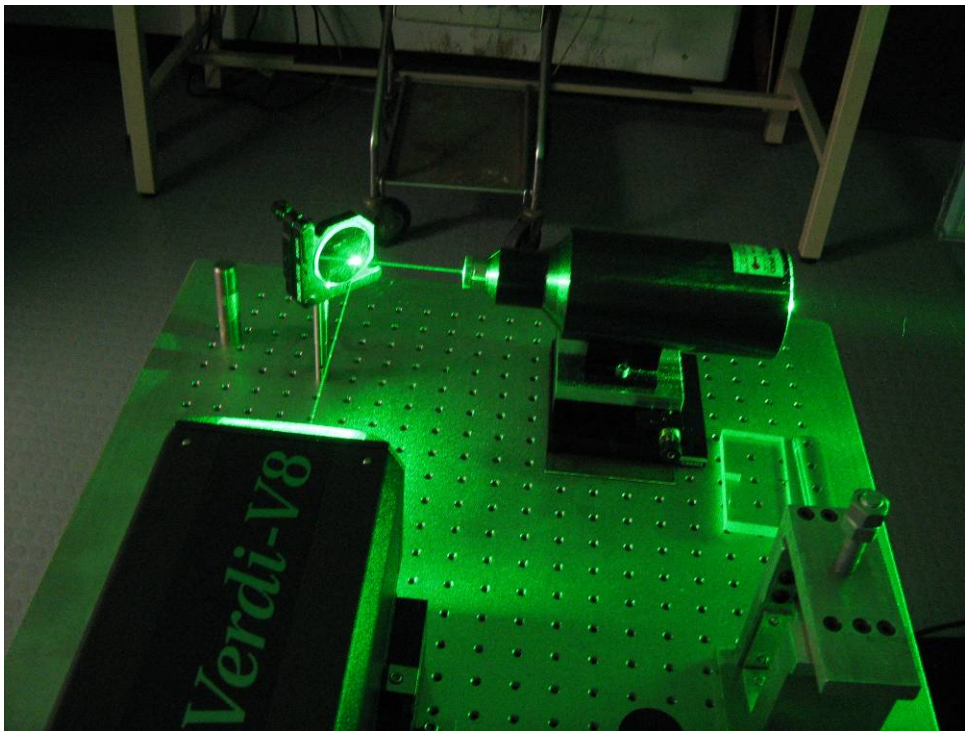

Figure A-7. Laser optics train. Mirror used to direct beam into beam expander.

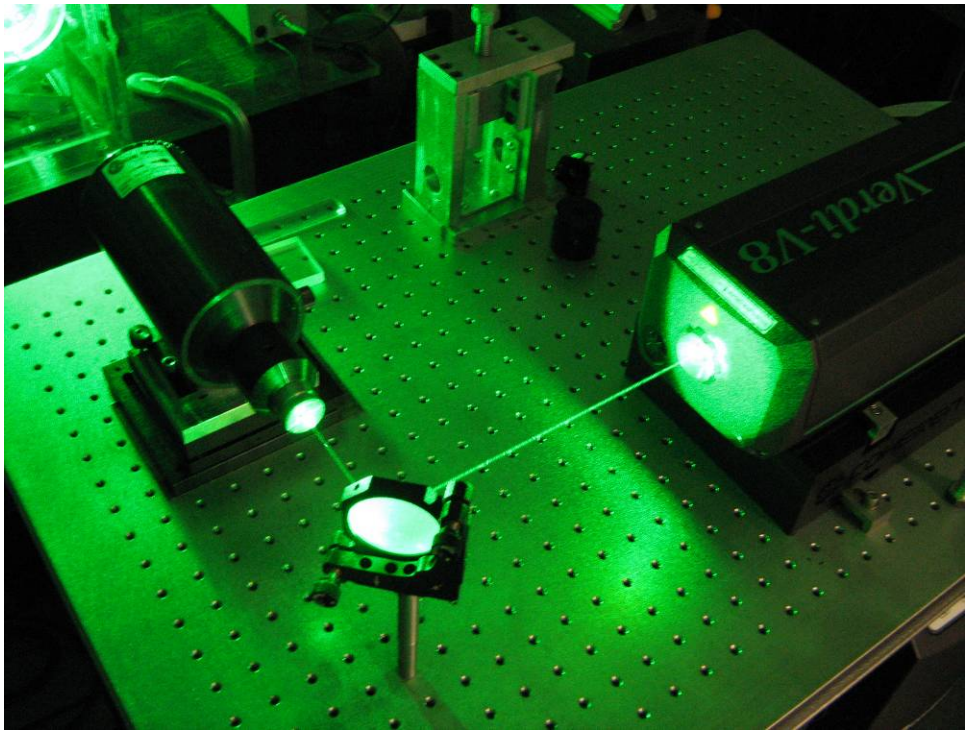

Figure A-8. Mirror adjusted to prevent retro-reflection from re-entering laser head.

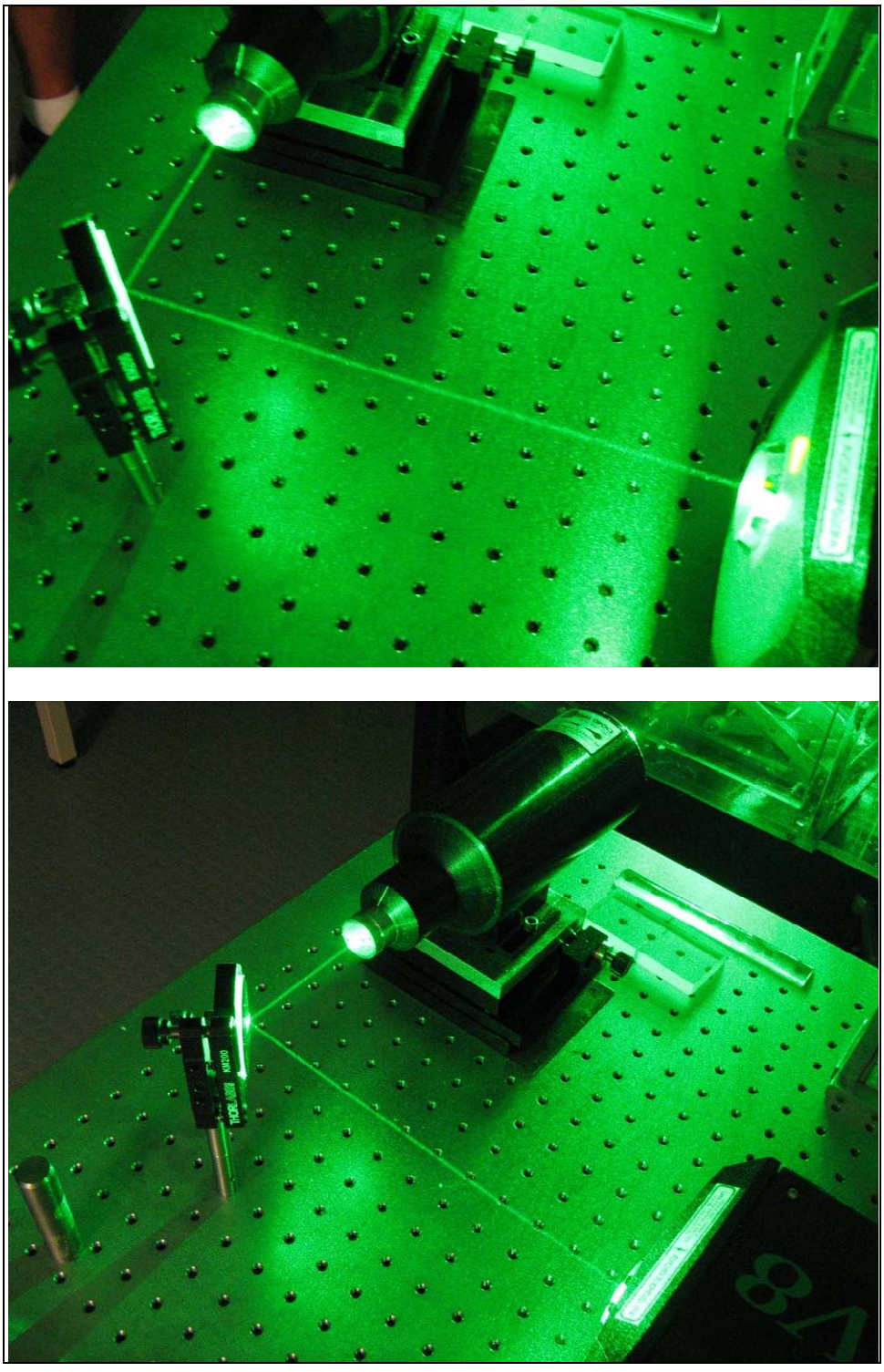

Figure A-9. Laser setup and alignment on incident optical table.

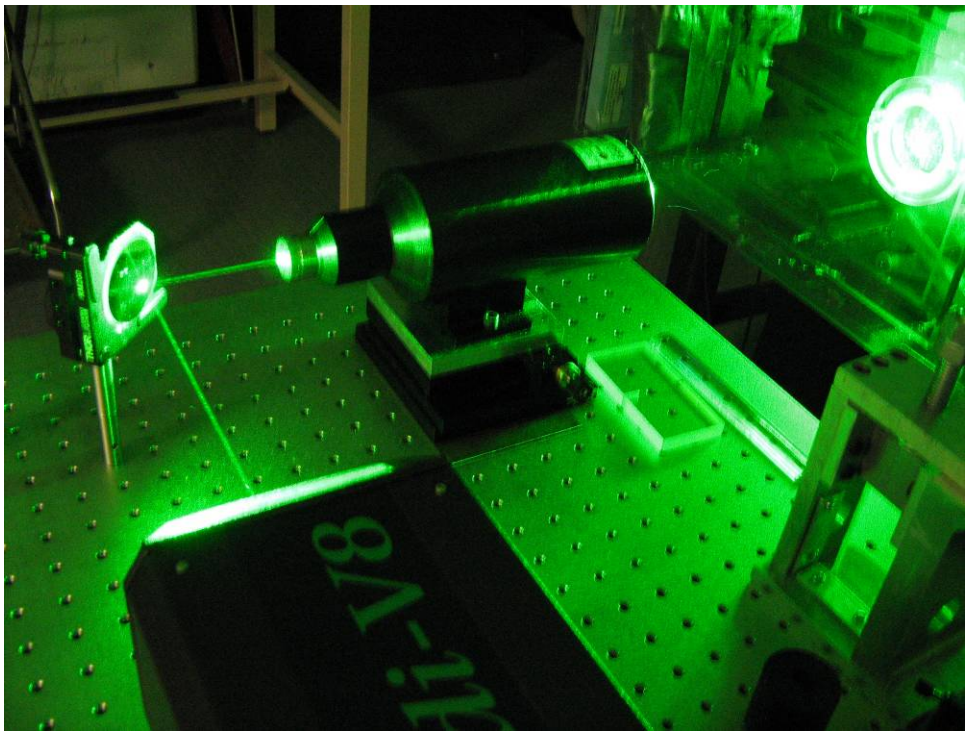

Figure A-10. Laser enters test chamber through 3-in antireflective window.

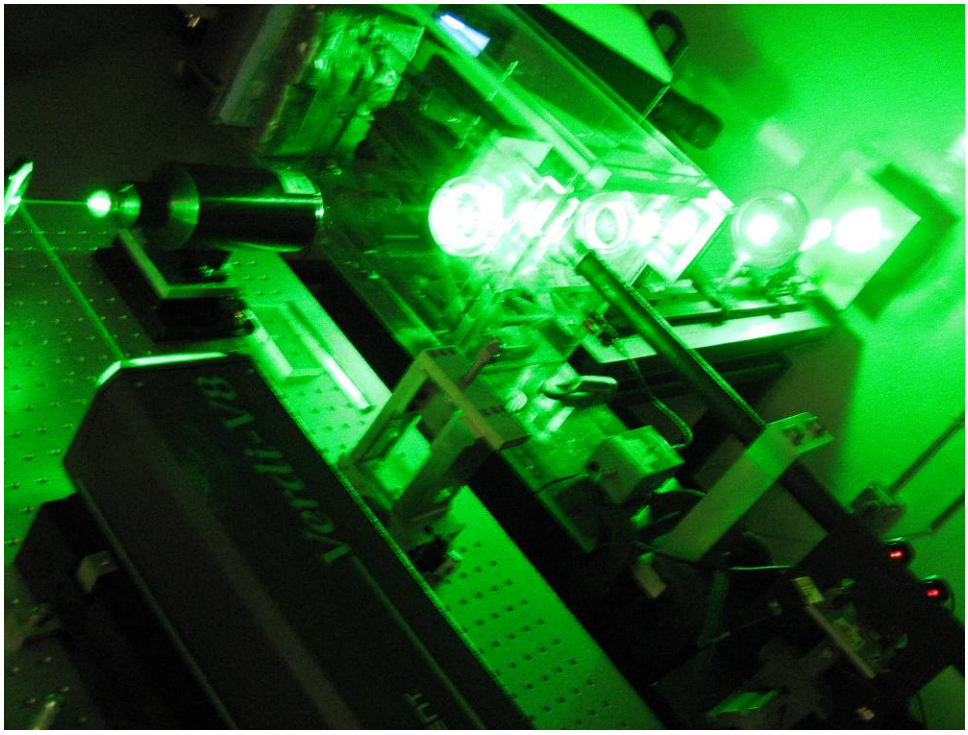

Figure A-11. Laser path through optical train. Windows are antireflective coated, and other optics are intentionally misaligned to prevent retroreflection.

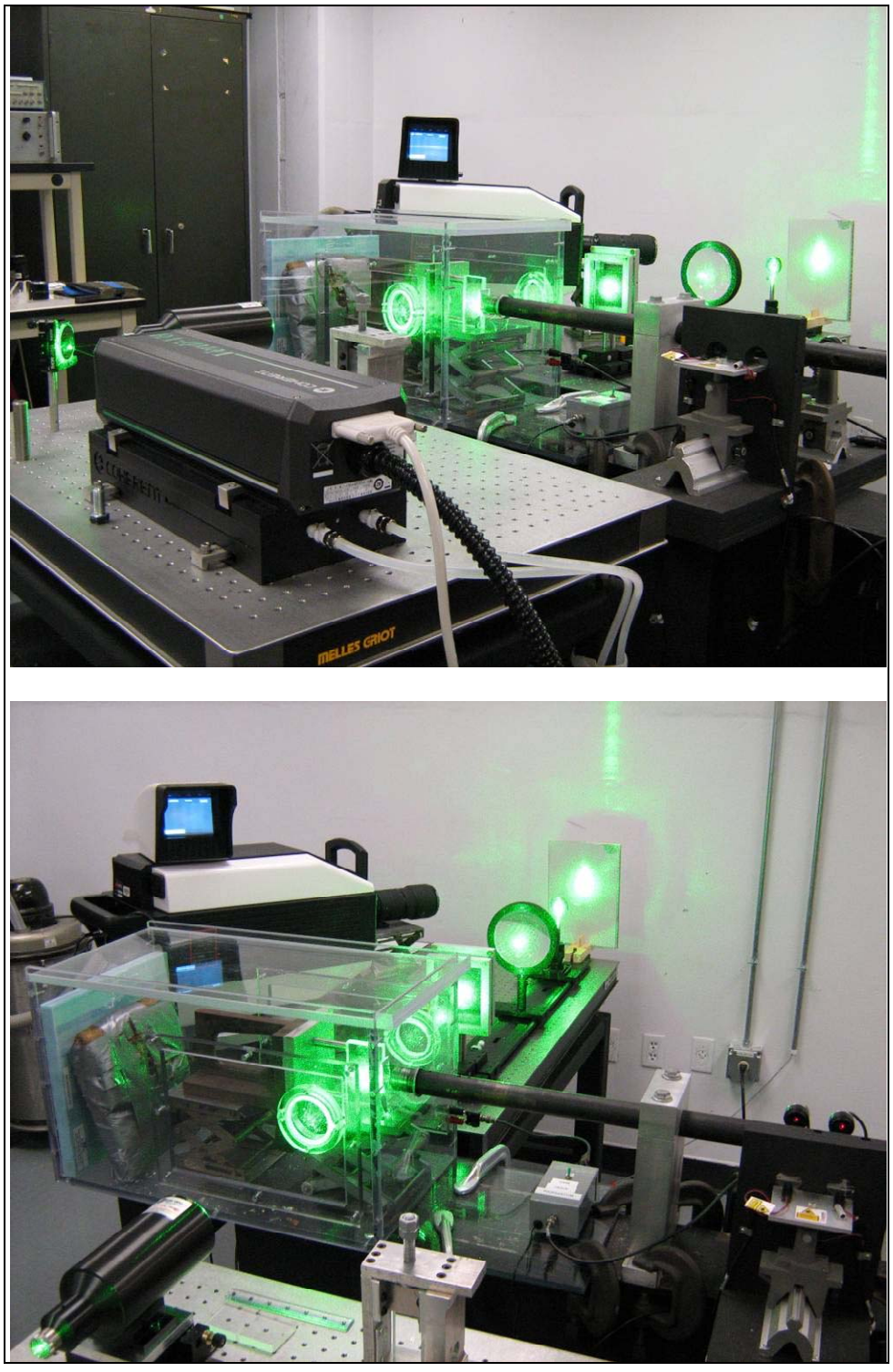

Figure A-12. Laser path through optical train showing high-speed camera positioned to observe screen.

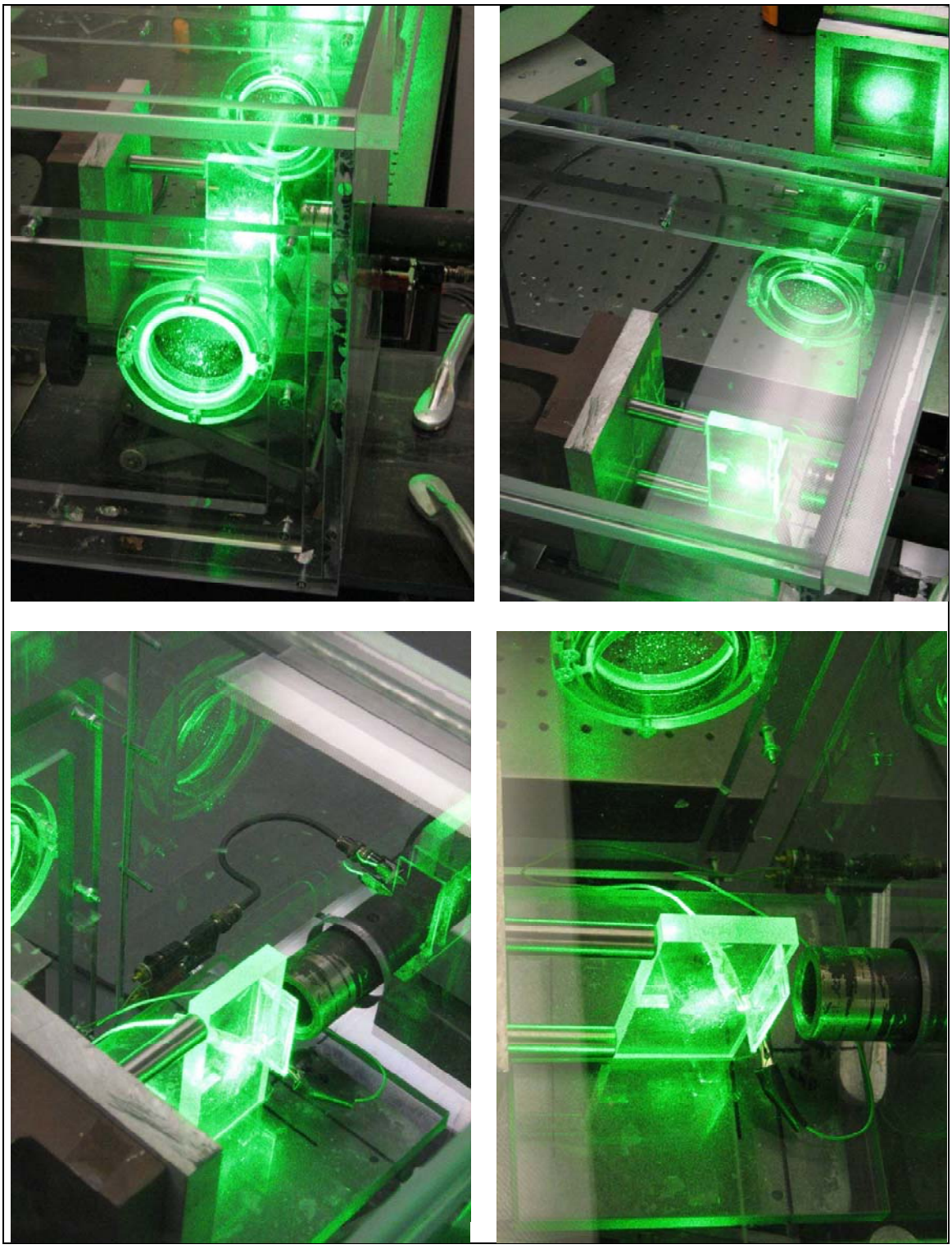

Figure A-13. Sample in three-point-bend configuration demonstrating alignment of laser illumination field with sample, target chamber, and defraction grating.

INTENTIONALLY LEFT BLANK.

Appendix B. Raw Shot Data

Table B-1. Shot parameters.

Shot	Pressure (psi)	Branching?	PMMA Target (in)	Projectile	Projectile Mass (g)
148	30	—	1/2 × 4 × 6	4-in Al	53
149	30	—	None	4-in Al	53
150	30	—	1/2 × 4 × 6	4-in Al	53
151	30	—	None	Thick Al	75
152	40	Y	1/2 × 4 × 6	Thick Al	75
153	40	Y	1/2 × 4 × 6	Thick Al	75
154	35	Y	1/2 × 4 × 6	Thick Al	72
155	35	—	1/2 × 4 × 6	Thick Al	73
156	35	Y	1/2 × 4 × 6	Thick Al	73
157	30	Y	1/2 × 4 × 6	Thick Al	73
158	35	—	None	Solid Al	67
159	30	Y	1/2 × 4 × 6	Solid Al	67
160	25	N	1/2 × 4 × 6	Solid Al	67
161	25	N	1/2 × 4 × 6	Solid Al	67
162	20	N	1/2 × 4 × 6	Solid Al	67
163	20	N	1/2 × 4 × 6	Solid Al	67
164	15	Y	1/2 × 4 × 6	Solid Al	67
165	15	N	1/2 × 4 × 6	Solid Al	67
166	15	N	1/2 × 4 × 6	Solid Al	67
167	10	N	1/2 × 4 × 6	Solid Al	67
168	10	N	1/2 × 4 × 6	Solid Al	67
169	5	—	1/2 × 4 × 6	Solid Al	67
170	5	N	1/2 × 4 × 6	Solid Al	67
171	5	N	1/2 × 4 × 6	Solid Al	67
172	30	Y	1/2 × 4 × 6	Solid Al	67
173	30	Y	1/2 × 4 × 6	Solid Al	67
174	25	Y	1/2 × 4 × 6	Solid Al	67
175	25	Y	1/2 × 4 × 6	Solid Al	67
176	25	N	1/2 × 4 × 6	Solid Al	67
177	25	N	1/2 × 4 × 6	Solid Al	67
178	20	N	1/2 × 4 × 6	Solid Al	67
179	27.5	Y	1/2 × 4 × 6	Solid Al	67
180	27.5	Y	1/2 × 4 × 6	Solid Al	67
181	27.5	Y	1/2 × 4 × 6	Solid Al	67
182	22.5	N	1/2 × 4 × 6	Solid Al	67
183	22.5	N	1/2 × 4 × 6	Solid Al	67
184	22.5	Y	1/2 × 4 × 6	Solid Al	67
185	40	Y	1/2 × 4 × 6	Solid Al	67
186	35	N	1/2 × 4 × 6	Solid Al	67
187	35	Y	1/2 × 4 × 6	Solid Al	67
188	20	Y?	1/2 × 4 × 6	Solid Al	67
189	15	N	1/2 × 4 × 6	Solid Al	67
190	10	N	1/2 × 4 × 6	Solid Al	67
191	5	N	1/2 × 4 × 6	Solid Al	67
192	5	N	1/2 × 4 × 6	Solid Al	67

Table B-2. Shot velocities and camera parameters.

Shot	t1-t2 (µs)	v1 (m/s)	Frames	Exposure Time (ns)	Frame Spacing (µs)	Trigger Delay (µs)	Total Time (µs)
148	936	67.84	16	500	3	45	53
149	971	65.40	—	—	—	—	113
150	970	65.46	16	500	7	75	—
151	1093	58.10	—	—	—	—	0
152	950	66.84	16	500	7	75	113
153	943	67.34	16	500	4	75	68
154	1003	63.31	16	500	4	75	68
155	1011	62.81	16	500	4	75	68
156	1055	60.19	16	500	4	70	68
157	1091	58.20	16	500	5	75	83
158	977	64.99	—	—	—	—	0
159	1047	60.65	16	500	5	75	83
160	1143	55.56	16	500	5	75	83
161	1140	55.70	16	500	5	75	83
162	1287	49.34	16	500	5	75	83
163	1287	49.34	16	500	5	75	83
164	1473	43.11	16	500	5	75	83
165	1482	42.85	16	500	5	75	83
166	1490	42.62	16	500	5	75	83
167	1850	34.32	16	500	6	75	98
168	1841	34.49	16	500	6	75	98
169	2833	22.41	16	500	6	75	98
170	2783	22.82	16	500	8	90	128
171	2858	22.22	16	500	8	90	128
172	1040	61.06	16	500	5	75	83
173	1043	60.88	16	1000	5	75	91
174	1137	55.85	16	1000	5	75	91
175	1130	56.19	16	1000	5	75	91
176	1130	56.19	16	1000	5	75	91
177	1130	56.19	16	1000	5	75	91
178	1262	50.32	16	1000	5	75	91
179	1080	58.80	16	1000	5	75	91
180	1087	58.42	16	1000	6	75	106
181	1090	58.26	16	1000	6	75	106
182	1210	52.48	16	1000	6	75	106
183	1303	48.73	16	1000	6	75	106
184	1203	52.78	16	1000	6	75	106
185	907	70.01	16	1000	4	75	76
186	963	65.94	16	1000	4	75	76
187	963	65.94	16	1000	5	75	91
188	1267	50.12	16	1000	5	75	91
189	1483	42.82	16	1000	6	75	106
190	1833	34.64	16	1000	6	90	106
191	2792	22.74	16	1000	6	90	106
192	2817	22.54	16	1000	8	100	136

INTENTIONALLY LEFT BLANK.

Appendix C. High-Speed Photos of Experiments

Figure C-1. Shot 63 – borosilicate glass.

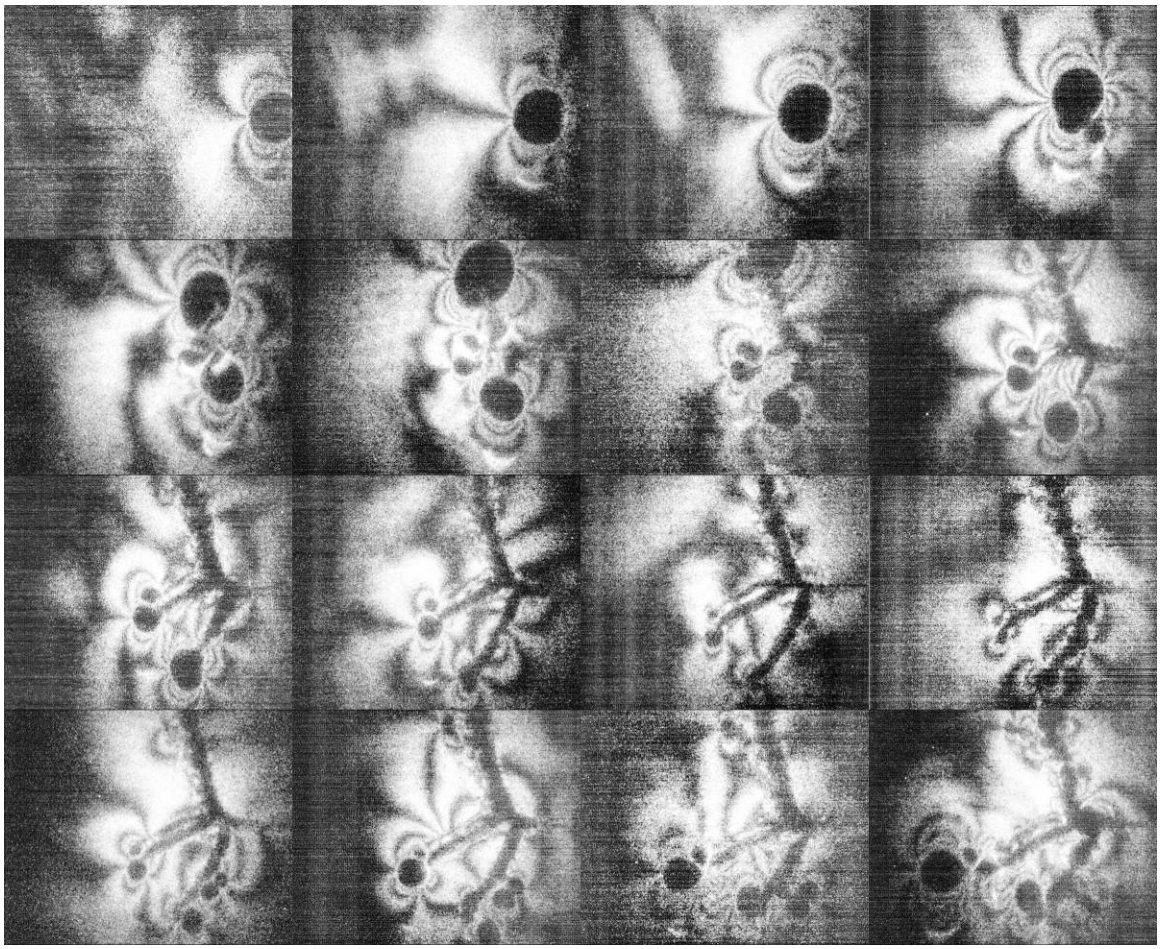

Figure C-2. Shot 152 – poly(methyl methacrylate) (PMMA).

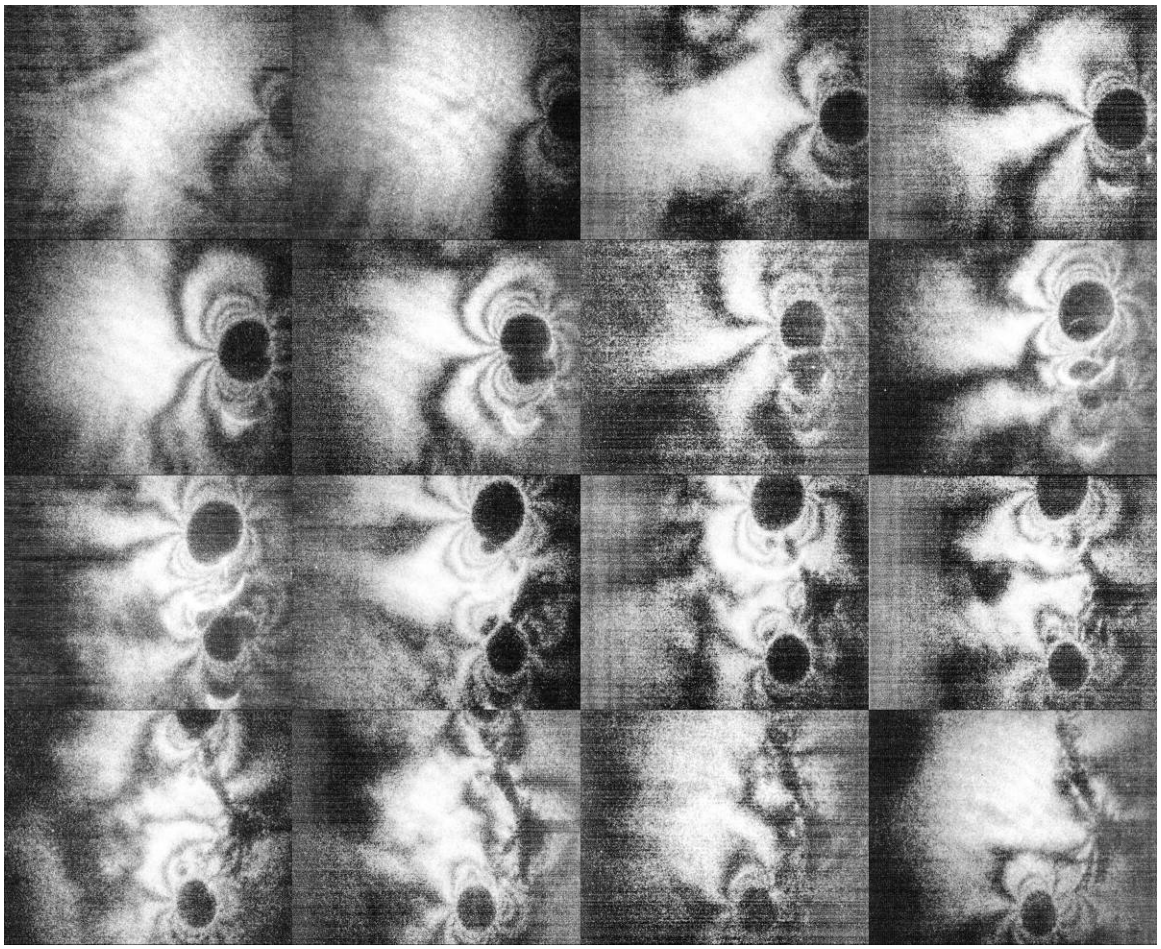

Figure C-3. Shot 153 – PMMA.

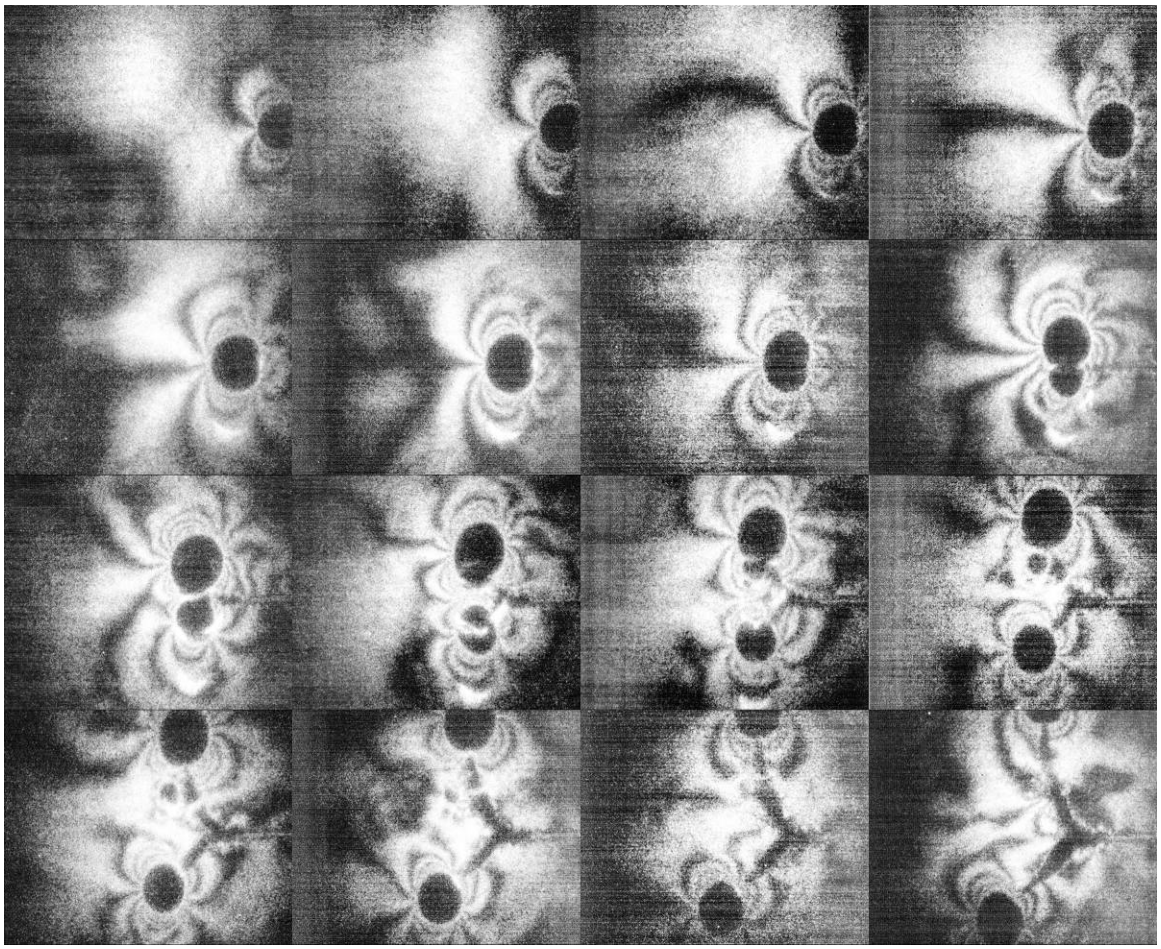

Figure C-4. Shot 154 – PMMA.

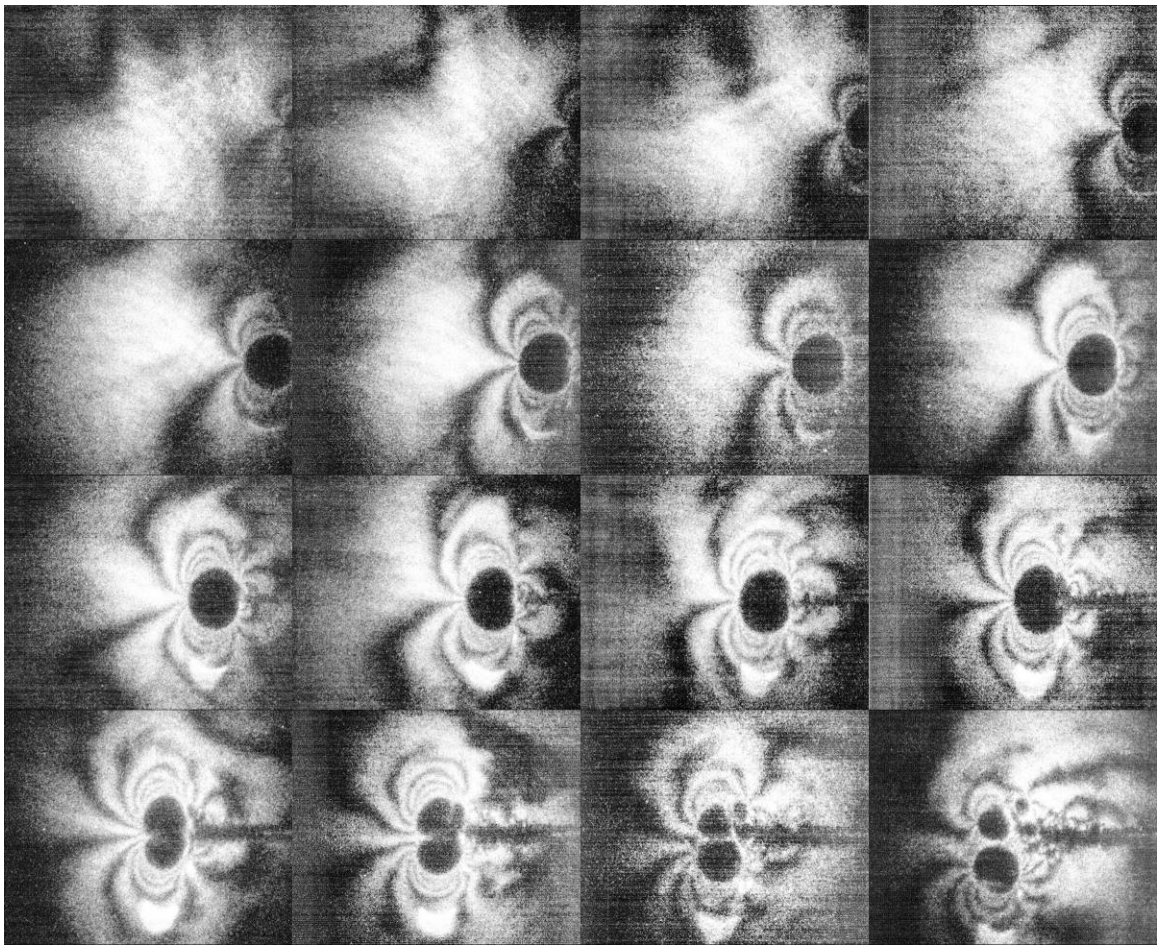

Figure C-5. Shot 156 – PMMA.

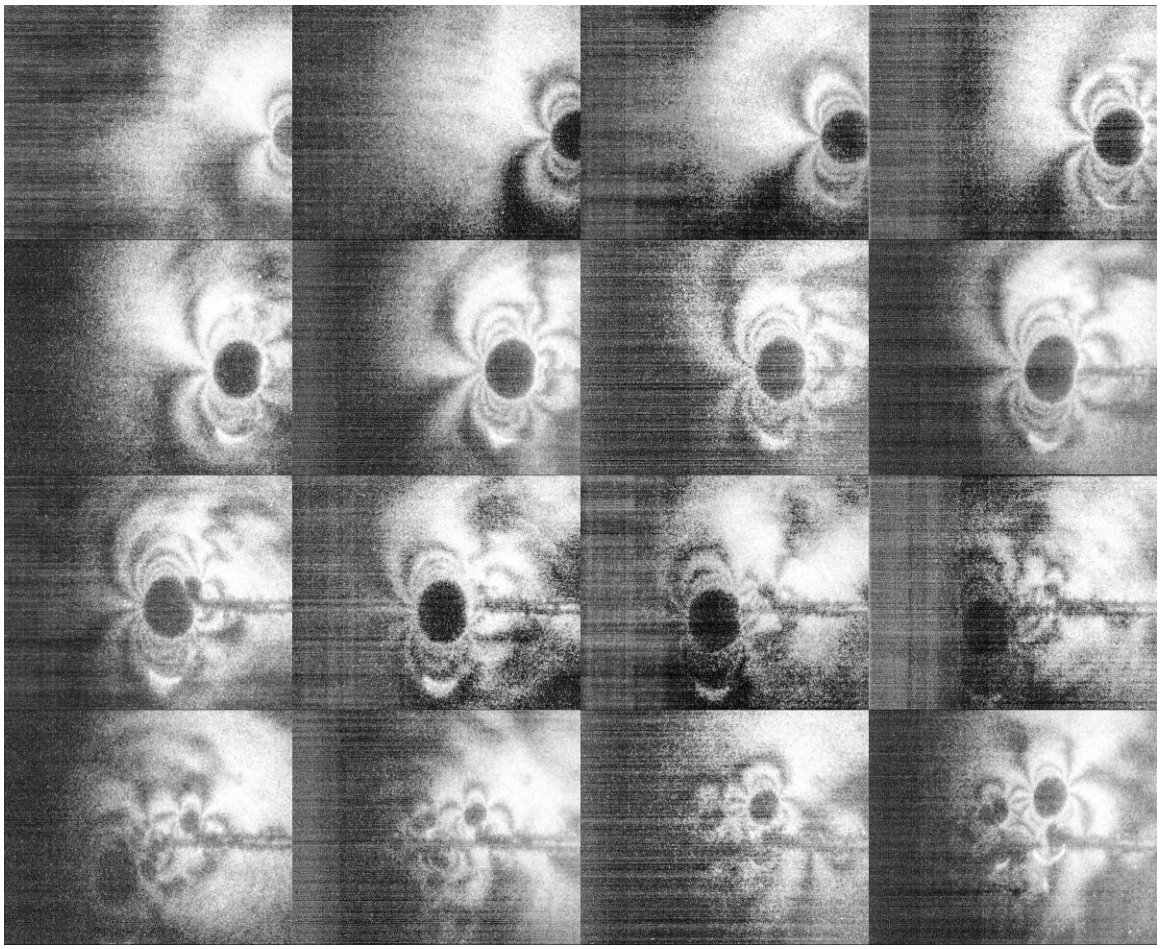

Figure C-6. Shot 157 – PMMA.

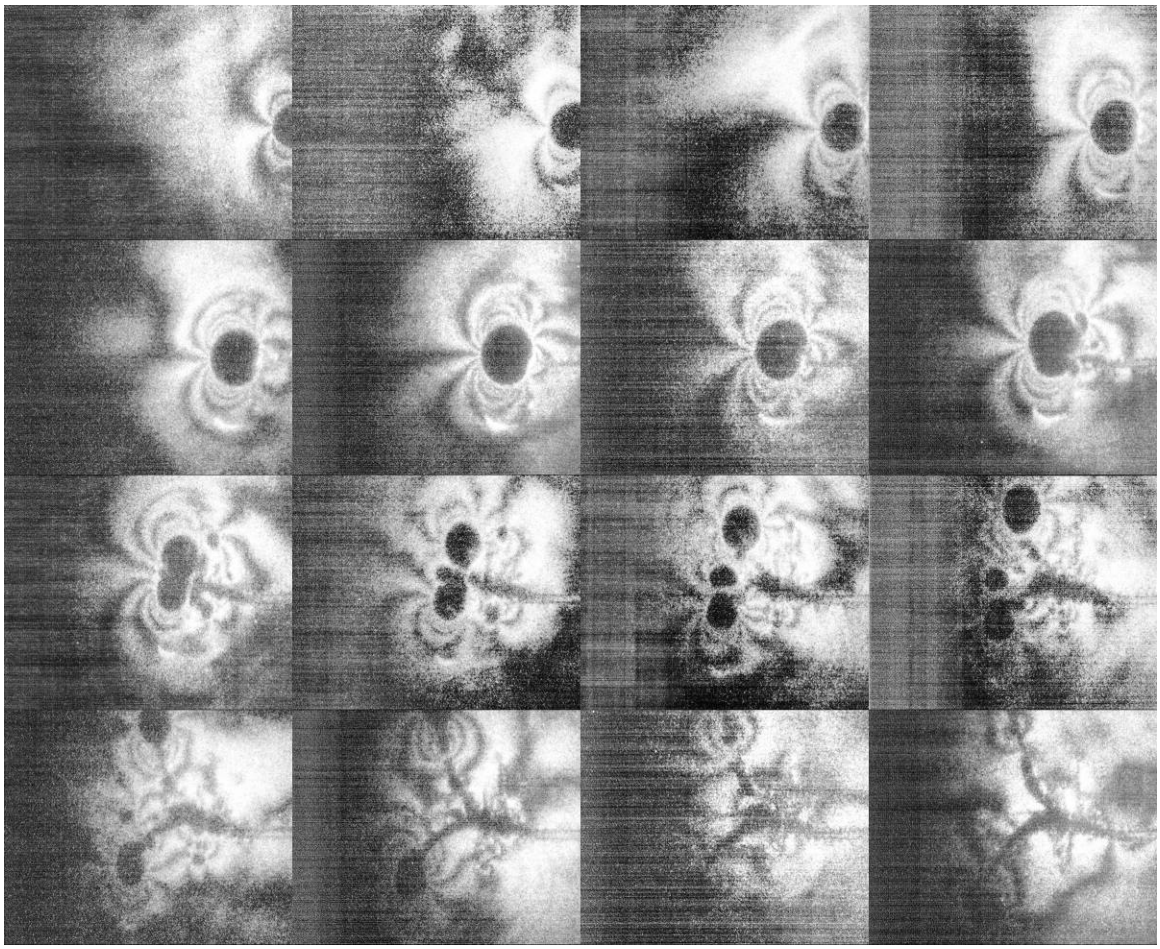

Figure C-7. Shot 159 – PMMA.

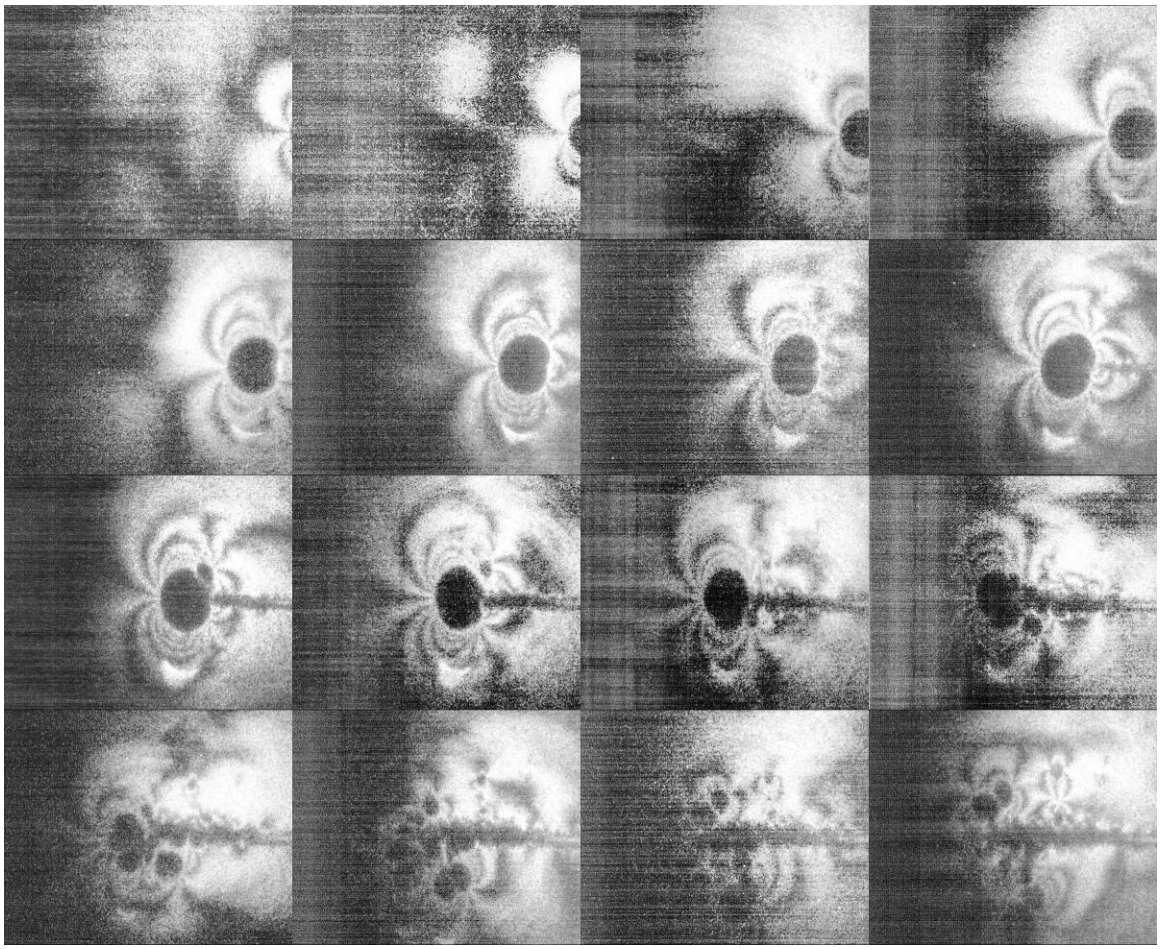

Figure C-8. Shot 160 – PMMA.

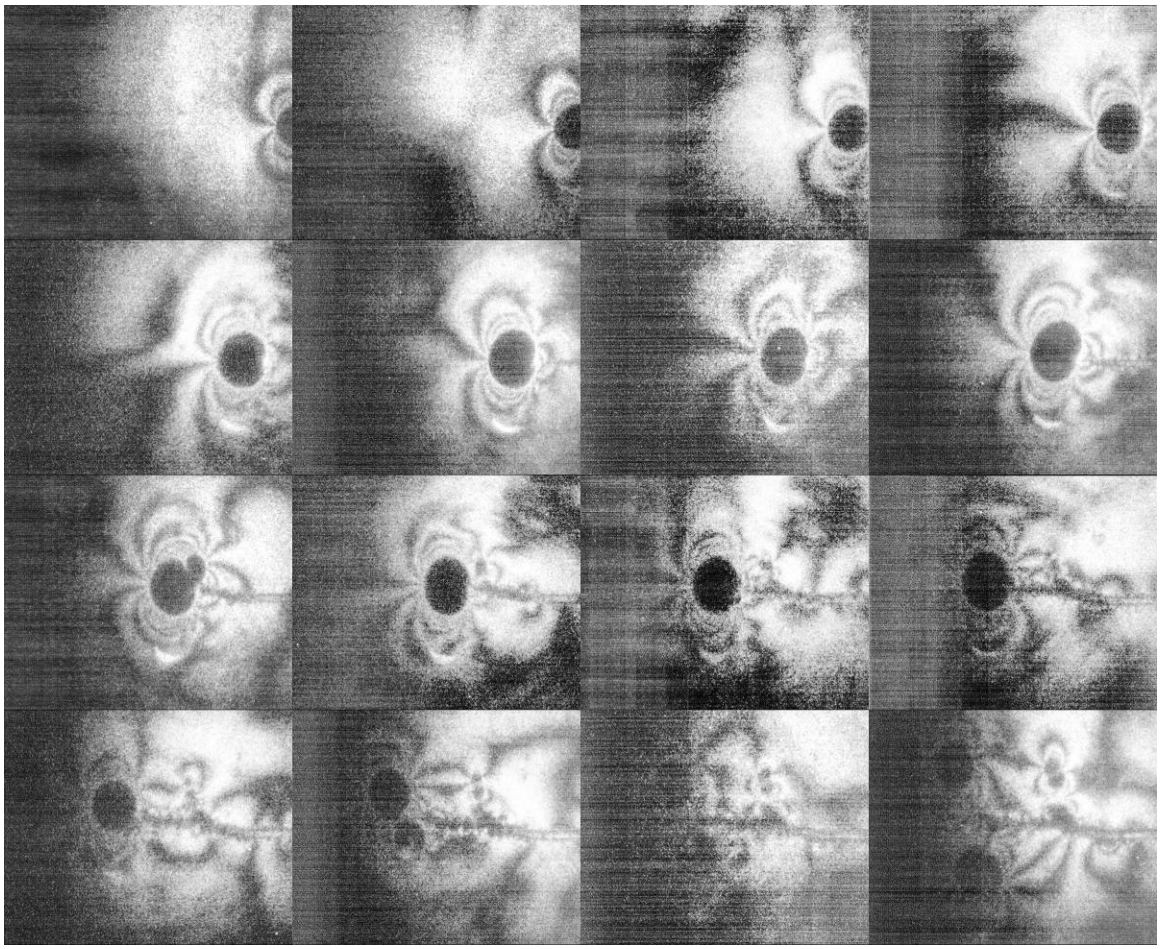

Figure C-9. Shot 161 – PMMA.

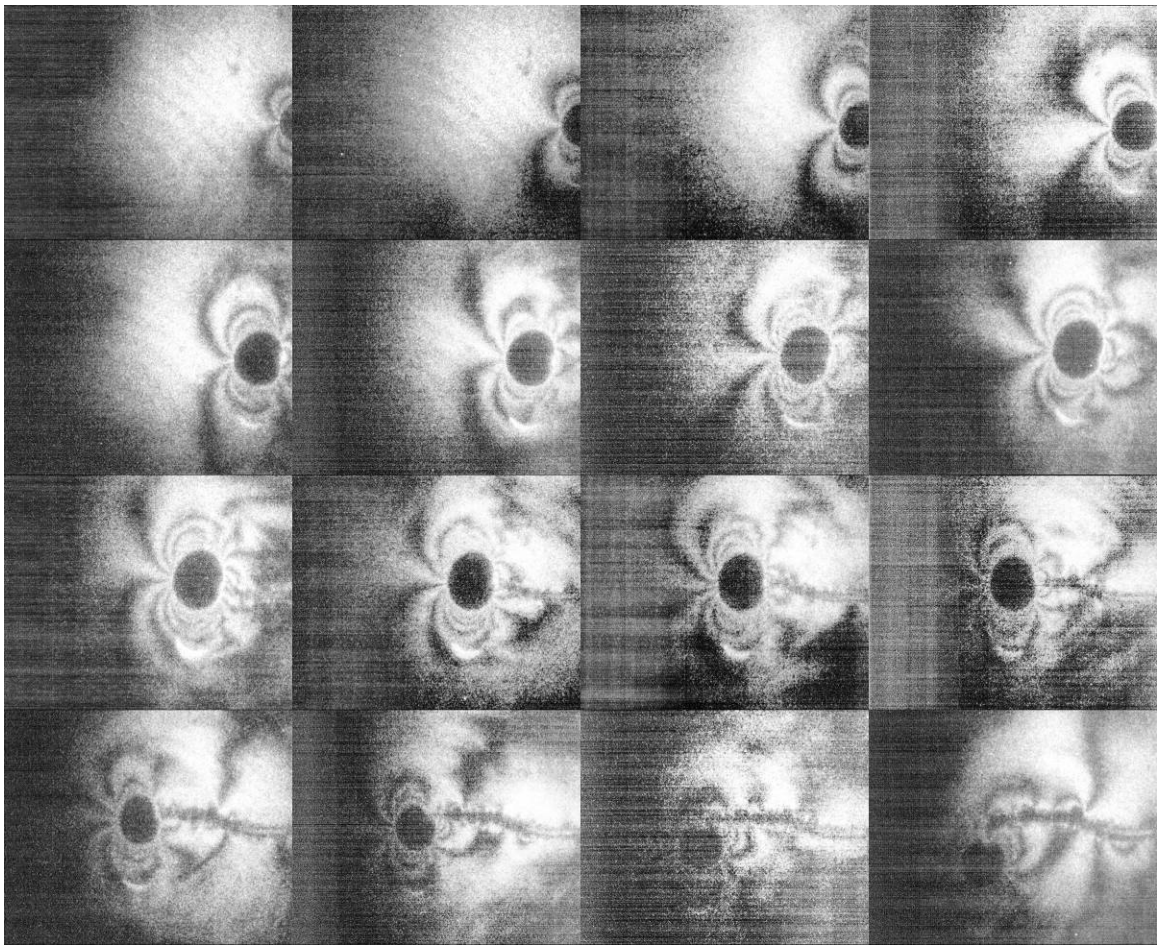

Figure C-10. Shot 162 – PMMA.

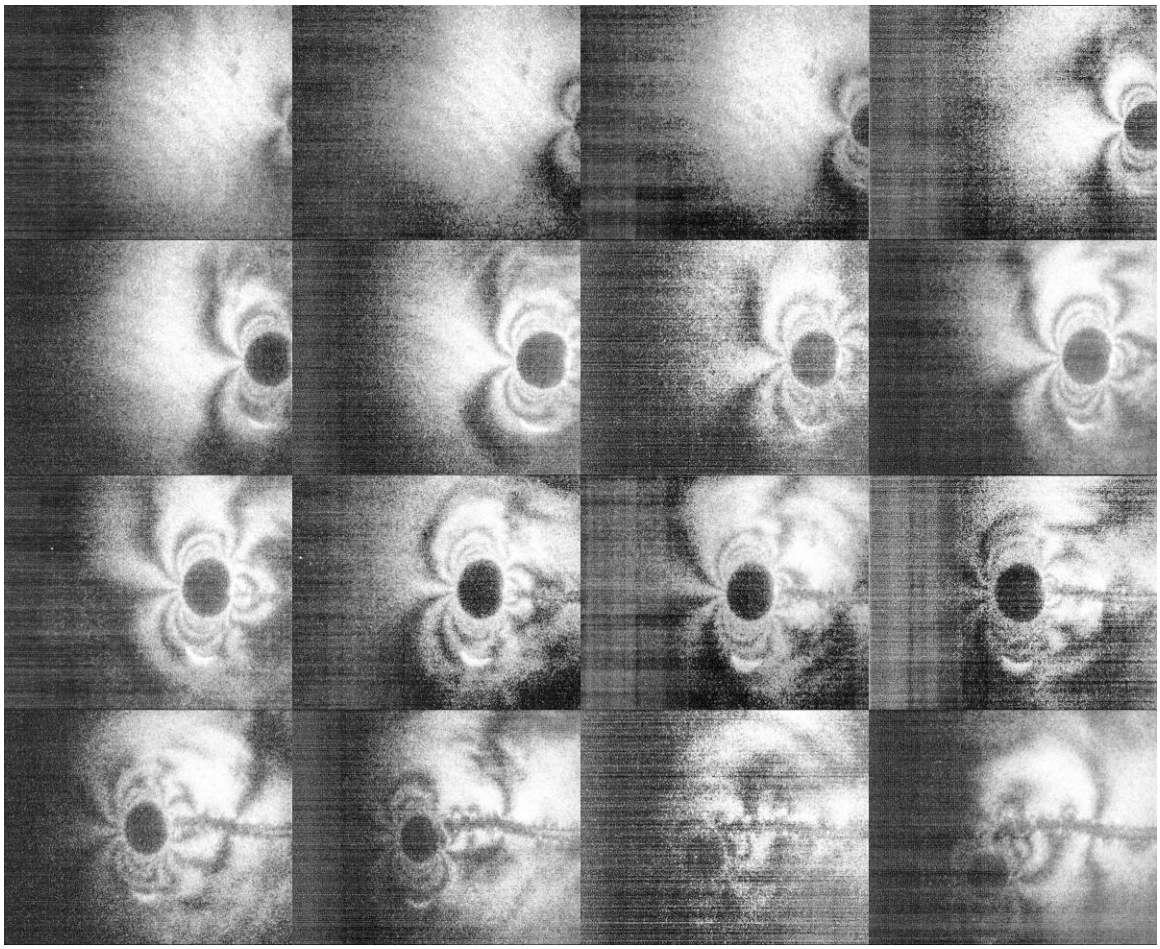

Figure C-11. Shot 163 – PMMA.

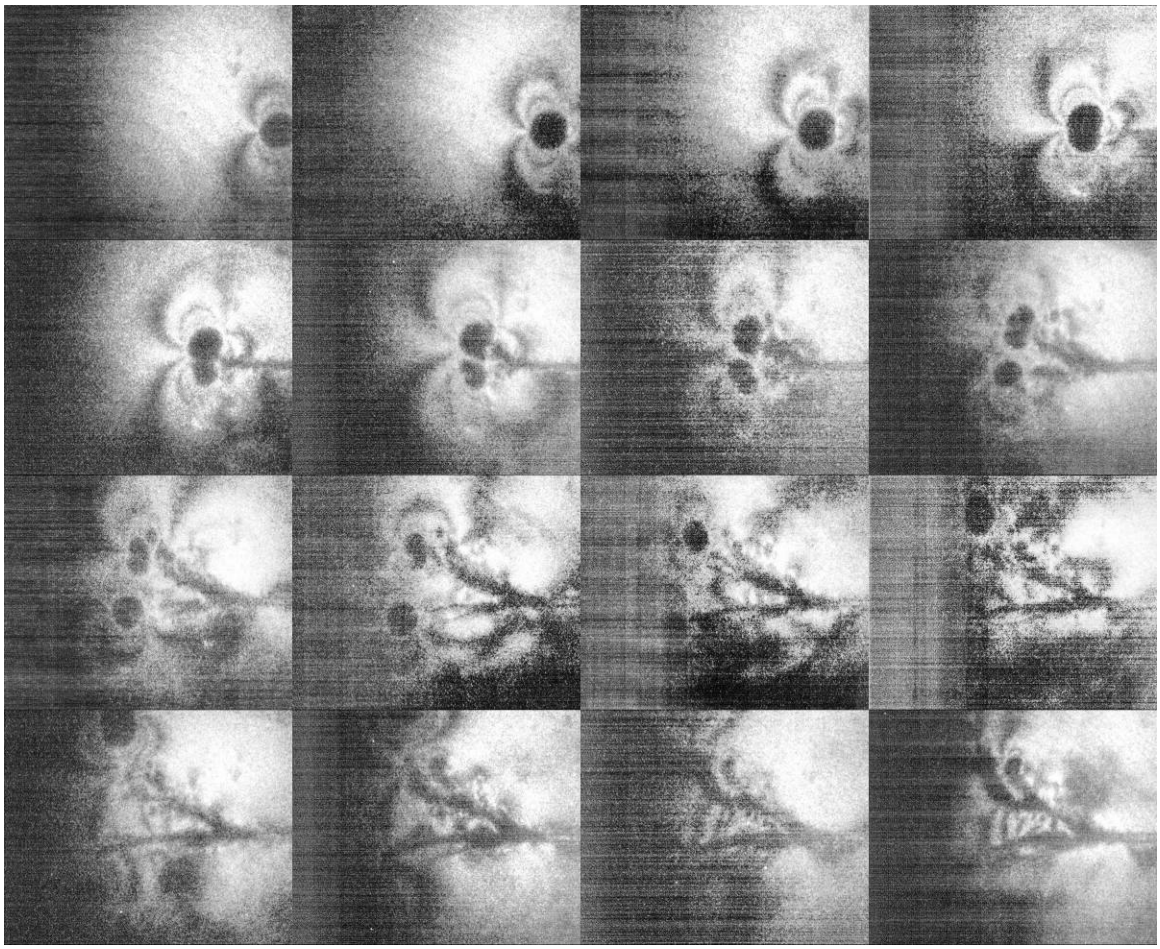

Figure C-12. Shot 164 – PMMA.

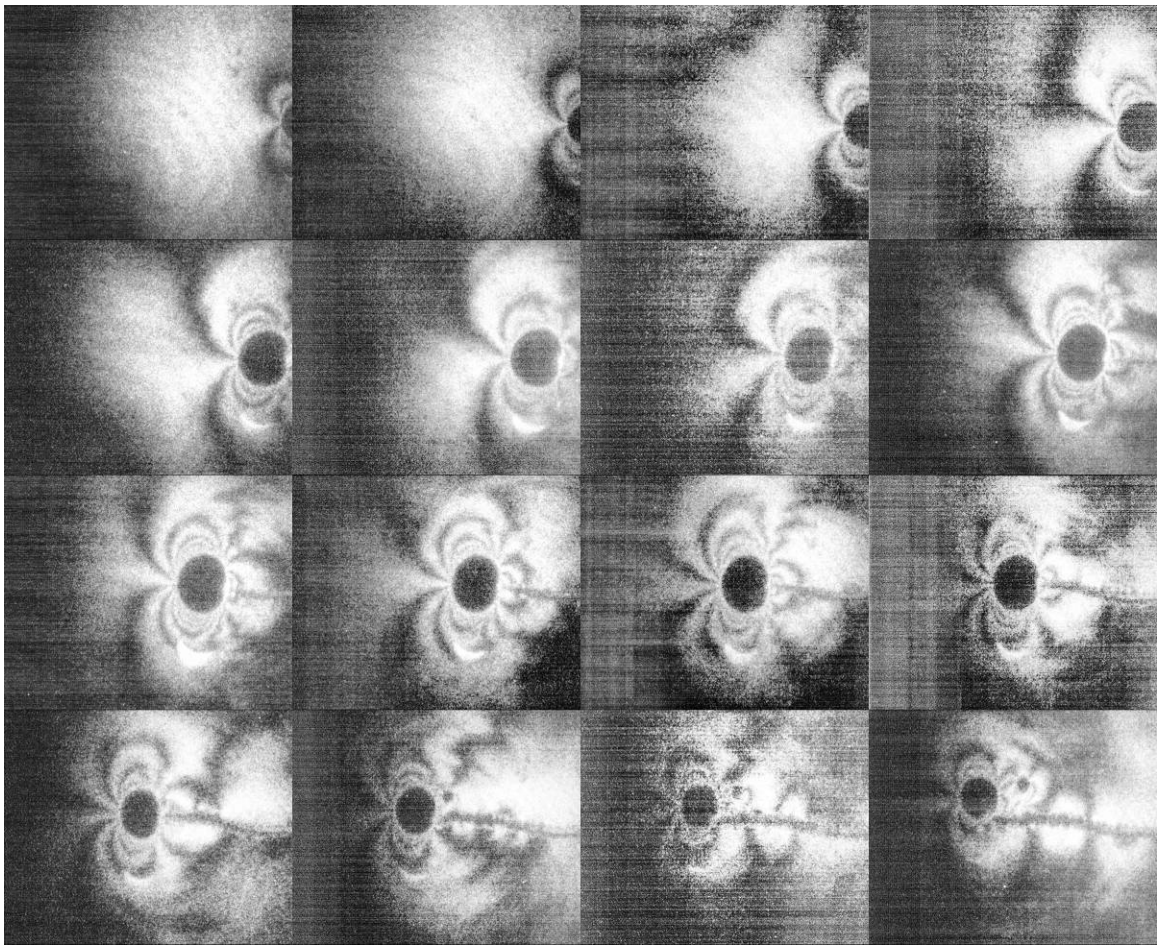

Figure C-13. Shot 165 – PMMA.

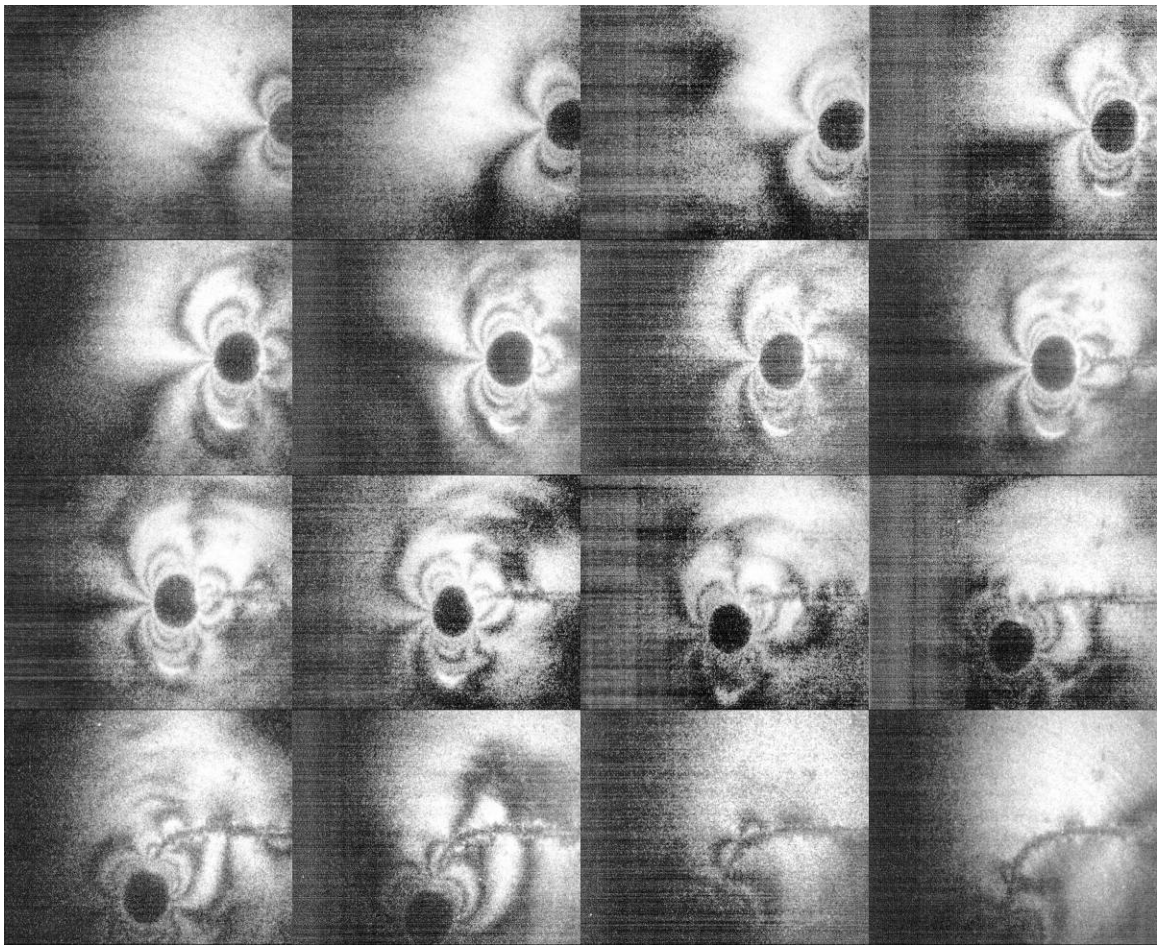

Figure C-14. Shot 166 – PMMA.

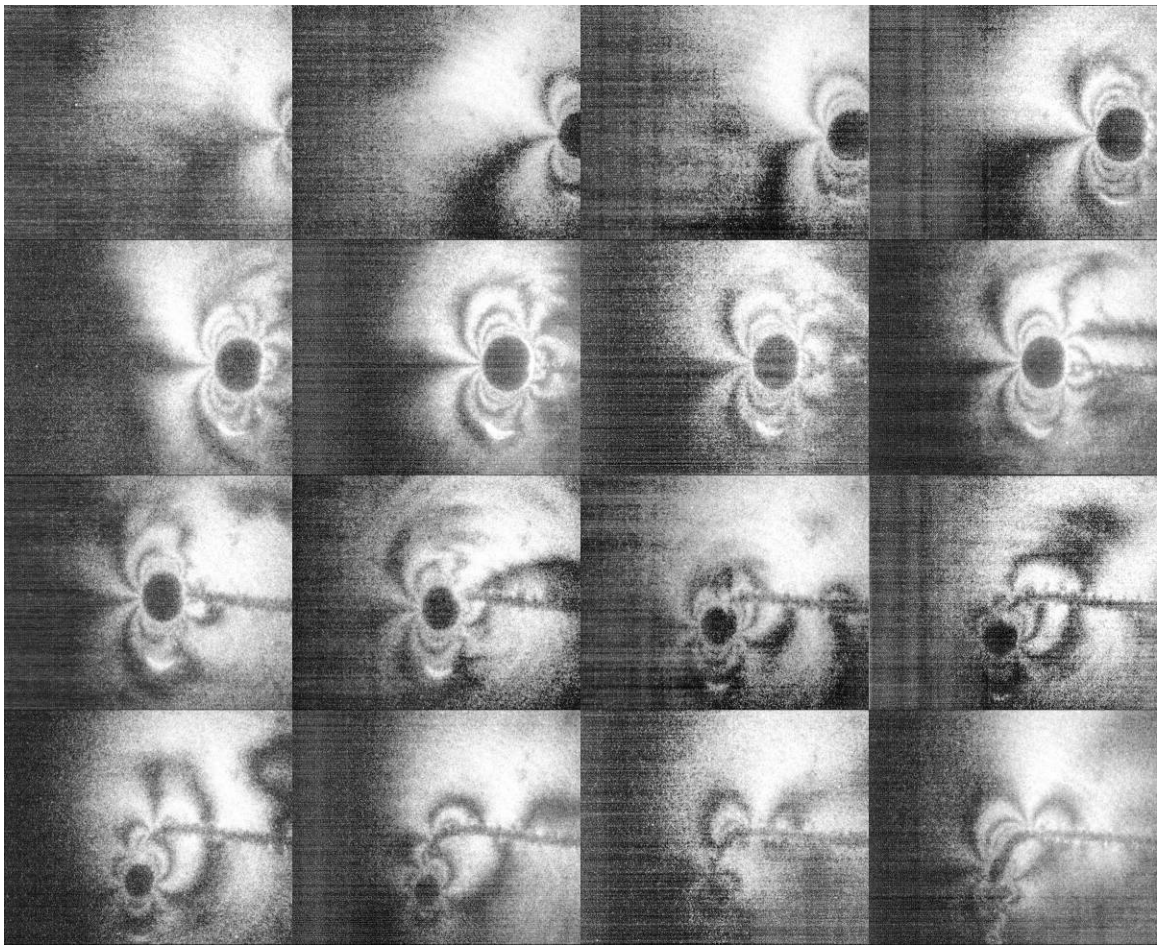

Figure C-15. Shot 167 – PMMA.

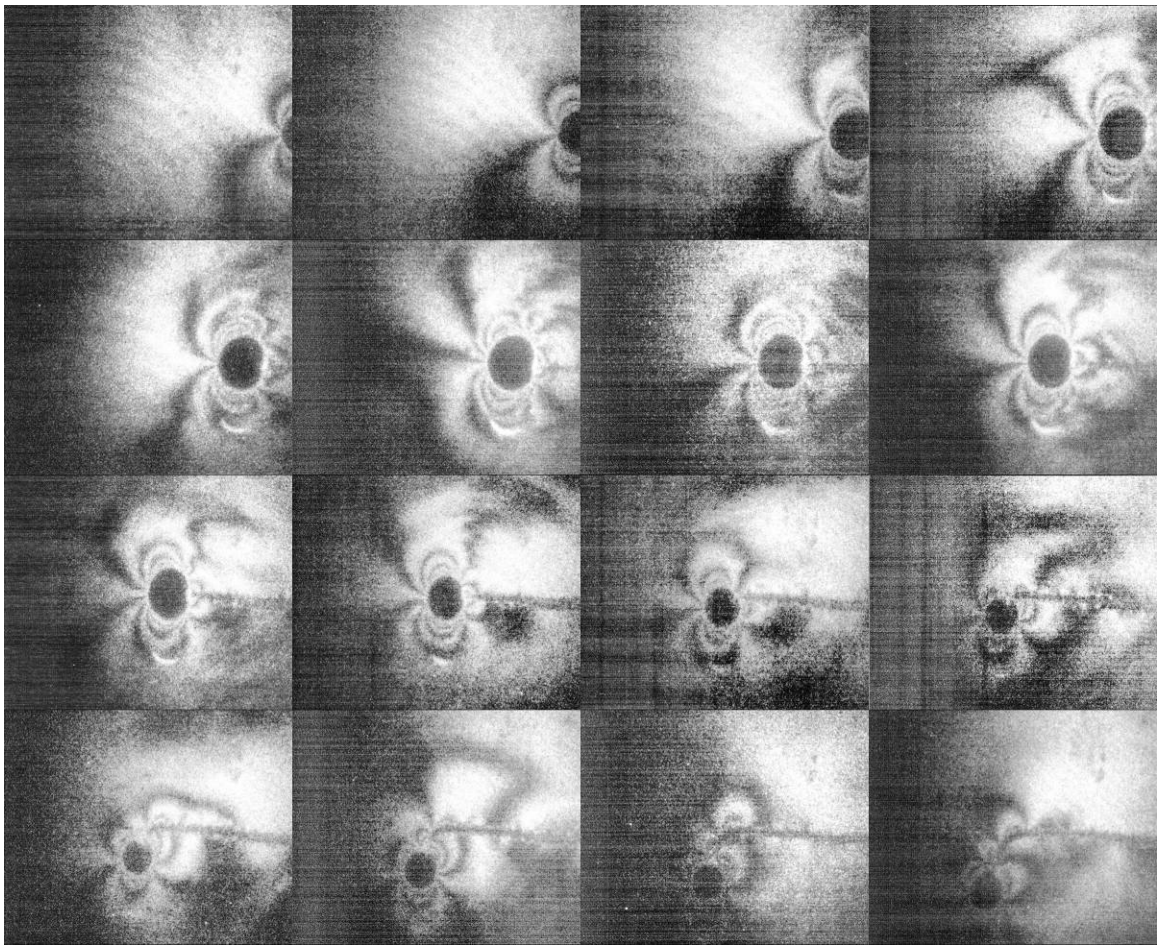

Figure C-16. Shot 168 – PMMA.

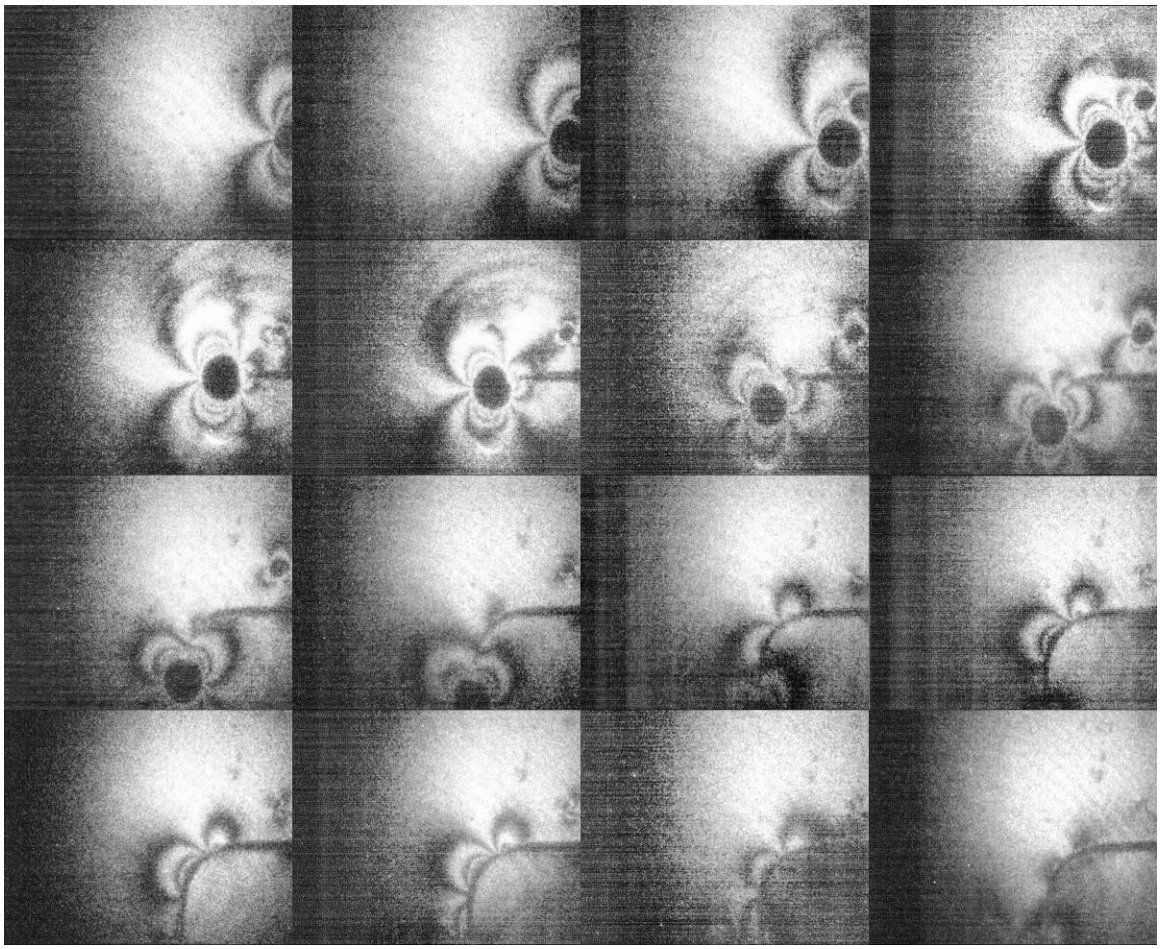

Figure C-17. Shot 170 – PMMA.

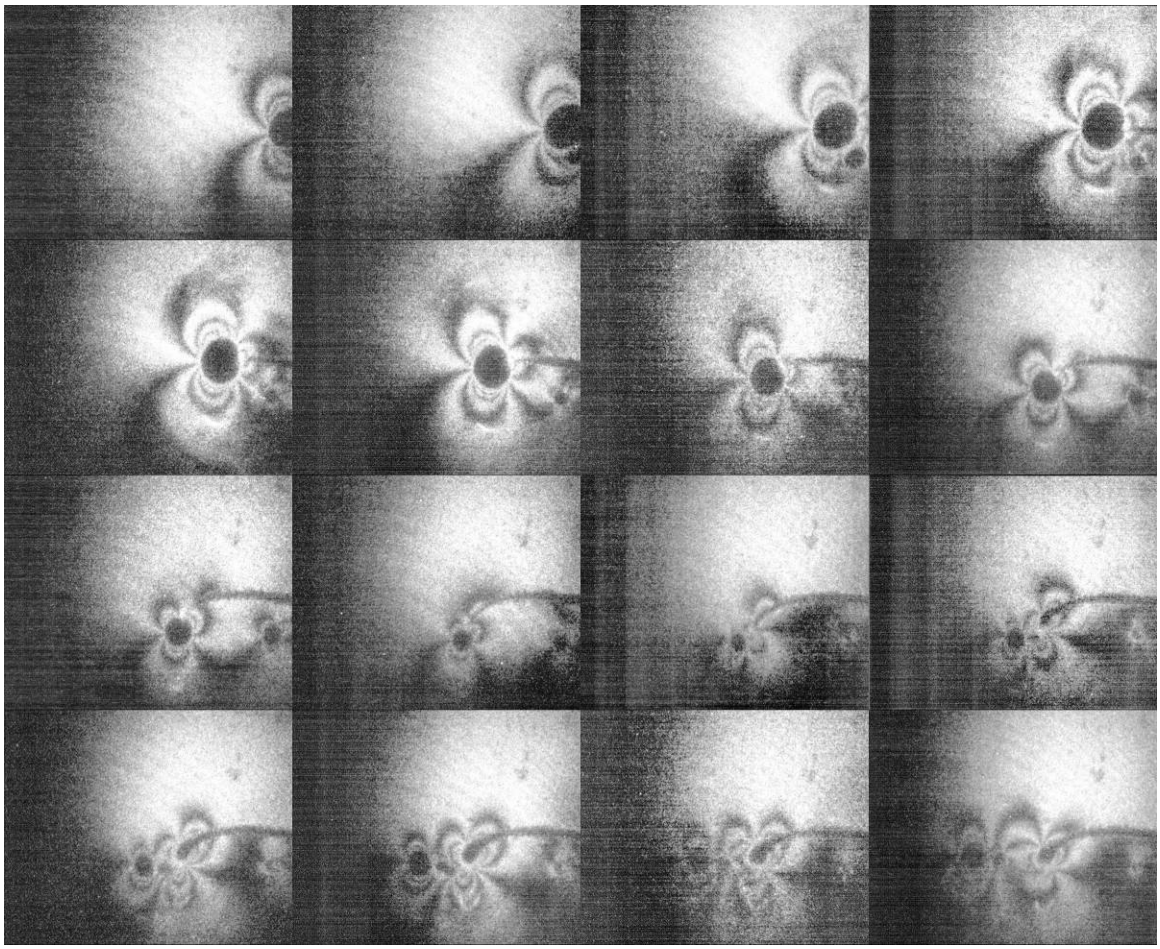

Figure C-18. Shot 171 – PMMA.

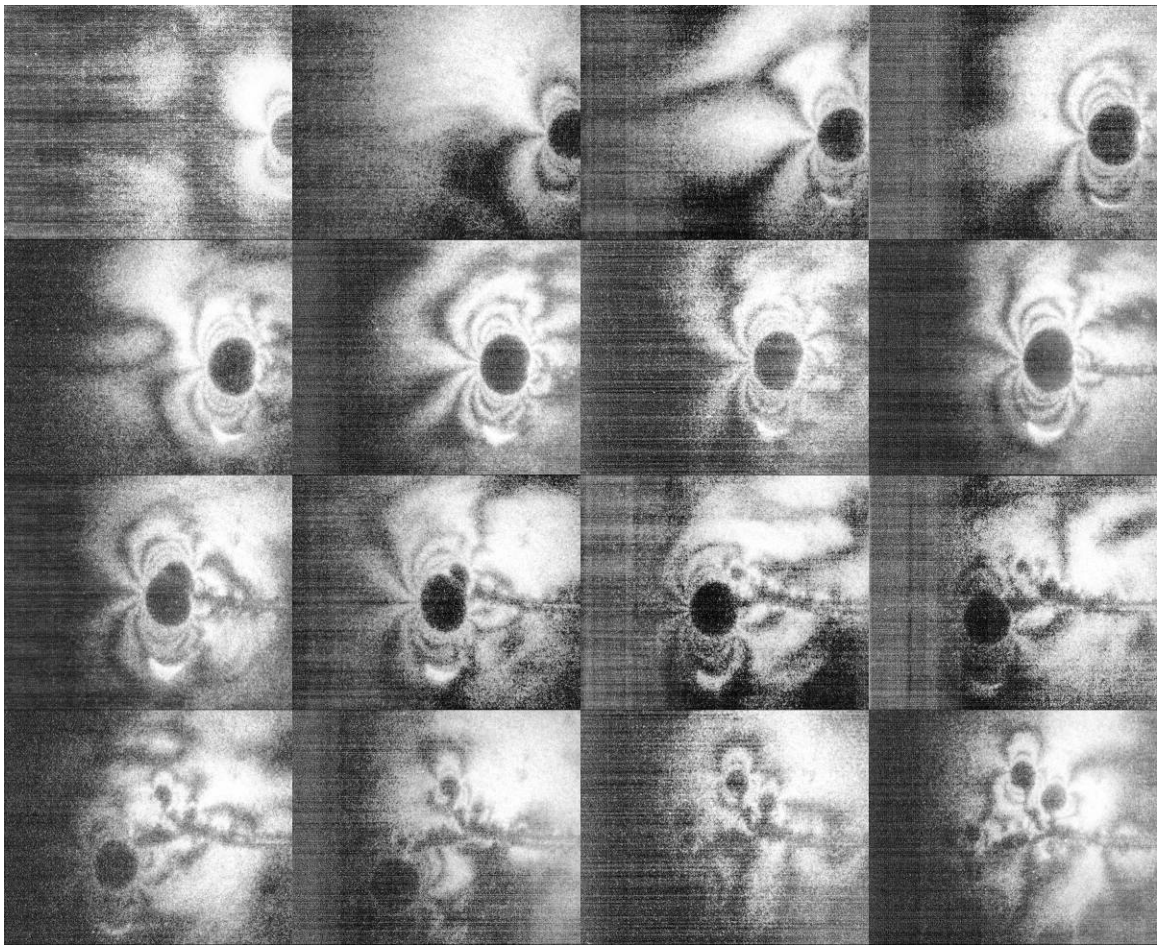

Figure C-19. Shot 172 – PMMA.

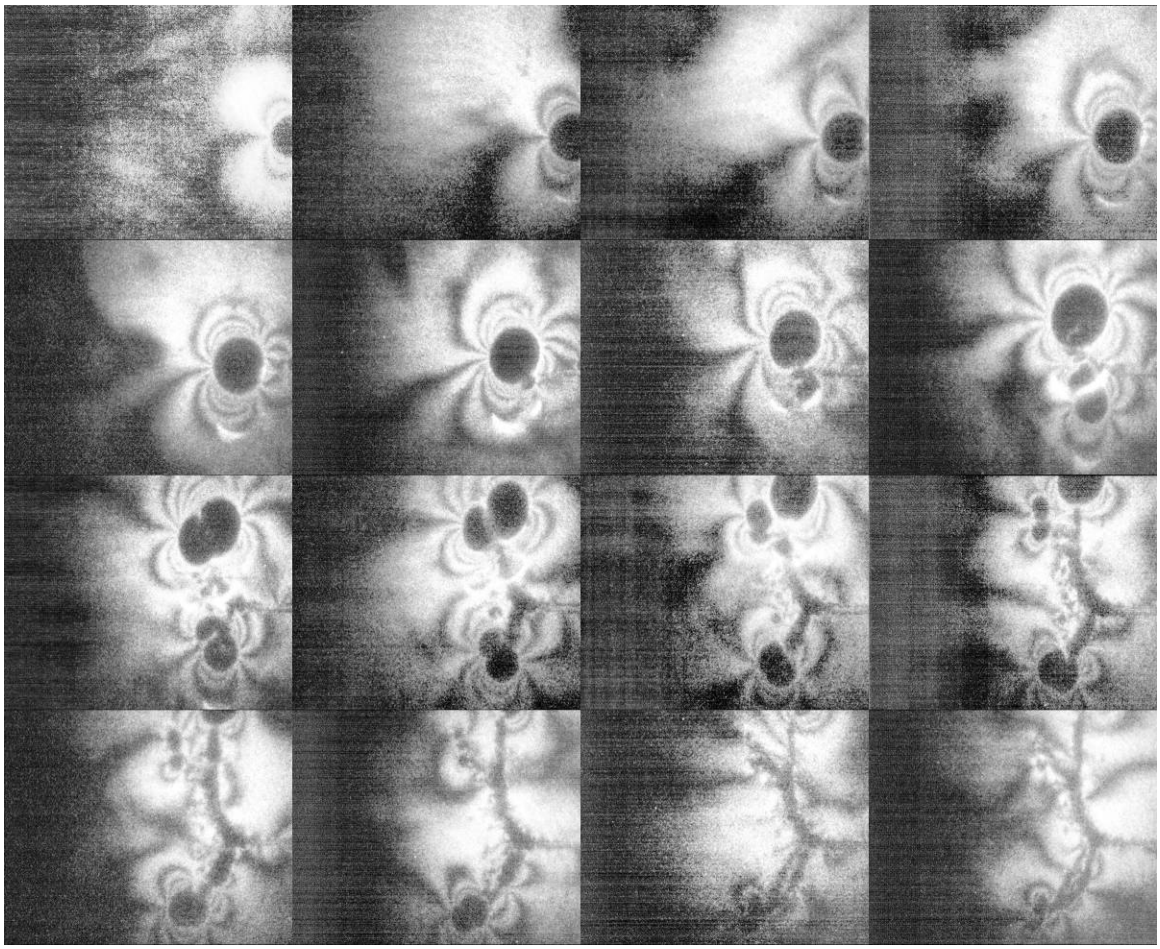

Figure C-20. Shot 173 – PMMA.

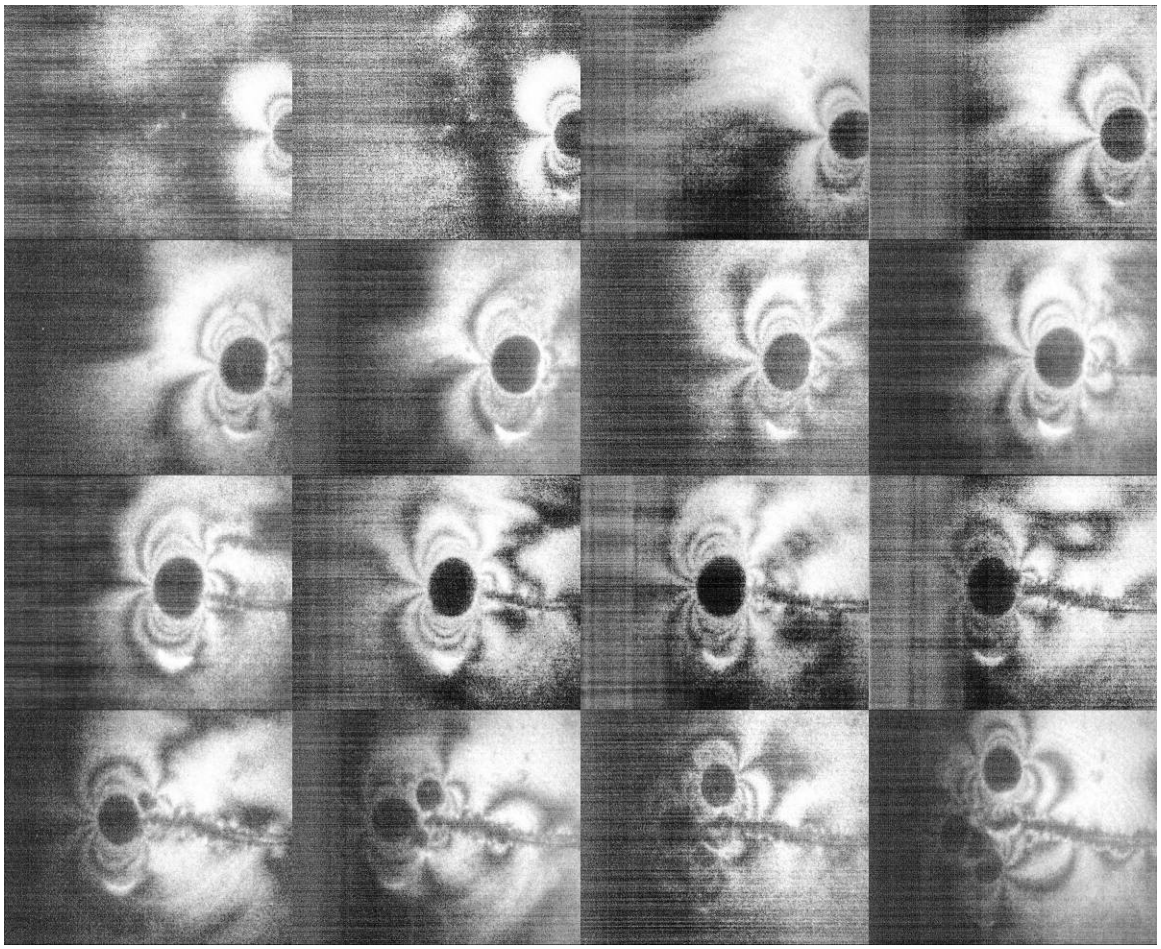

Figure C-21. Shot 174 – PMMA.

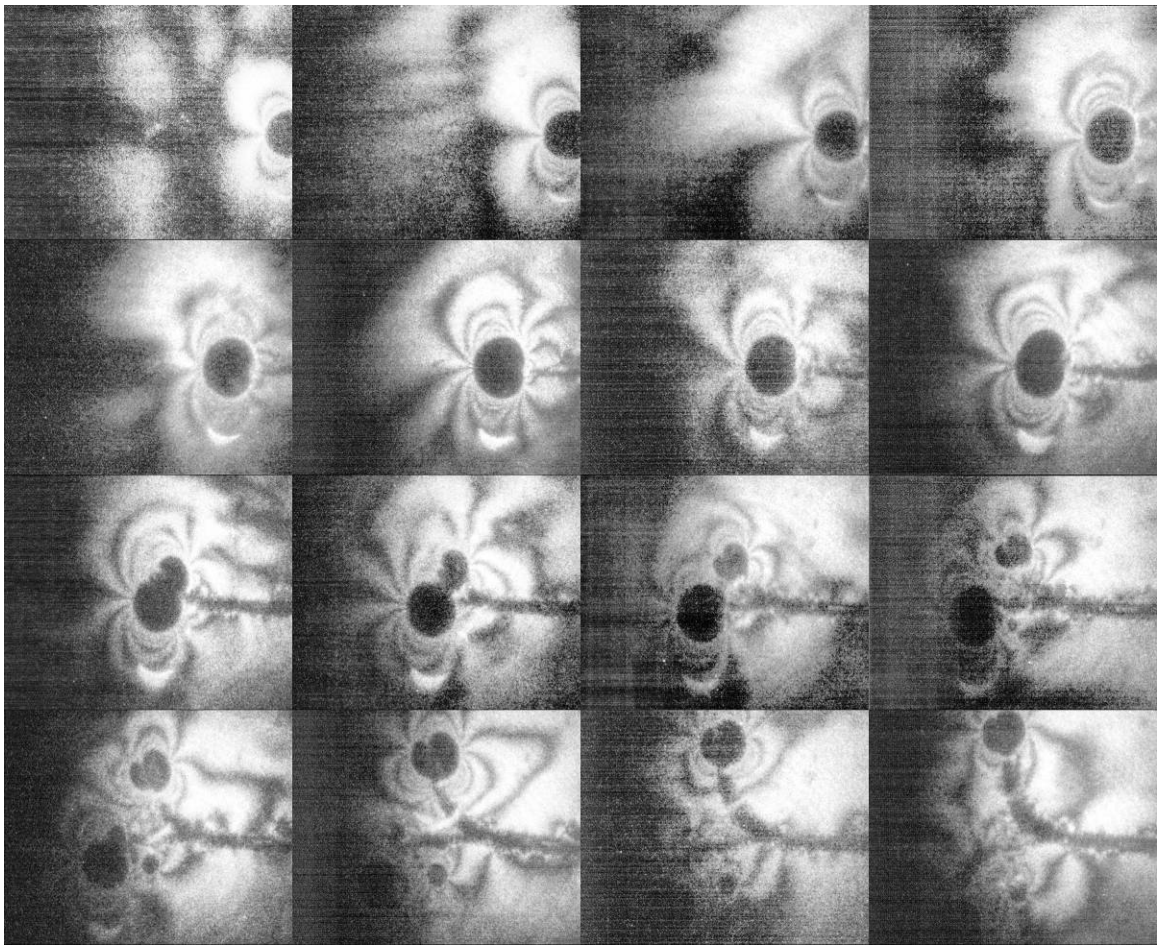

Figure C-22. Shot 175 – PMMA.

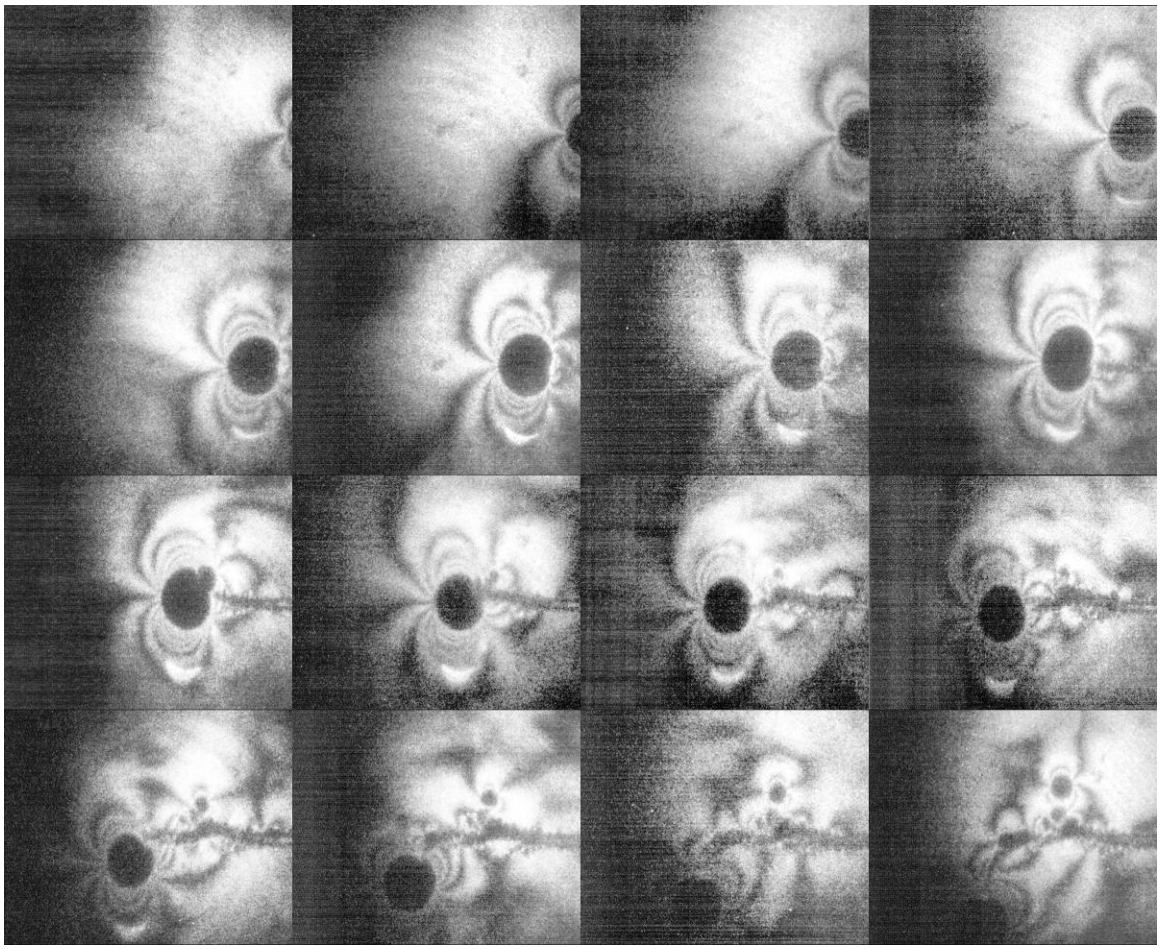

Figure C-23. Shot 176 – PMMA.

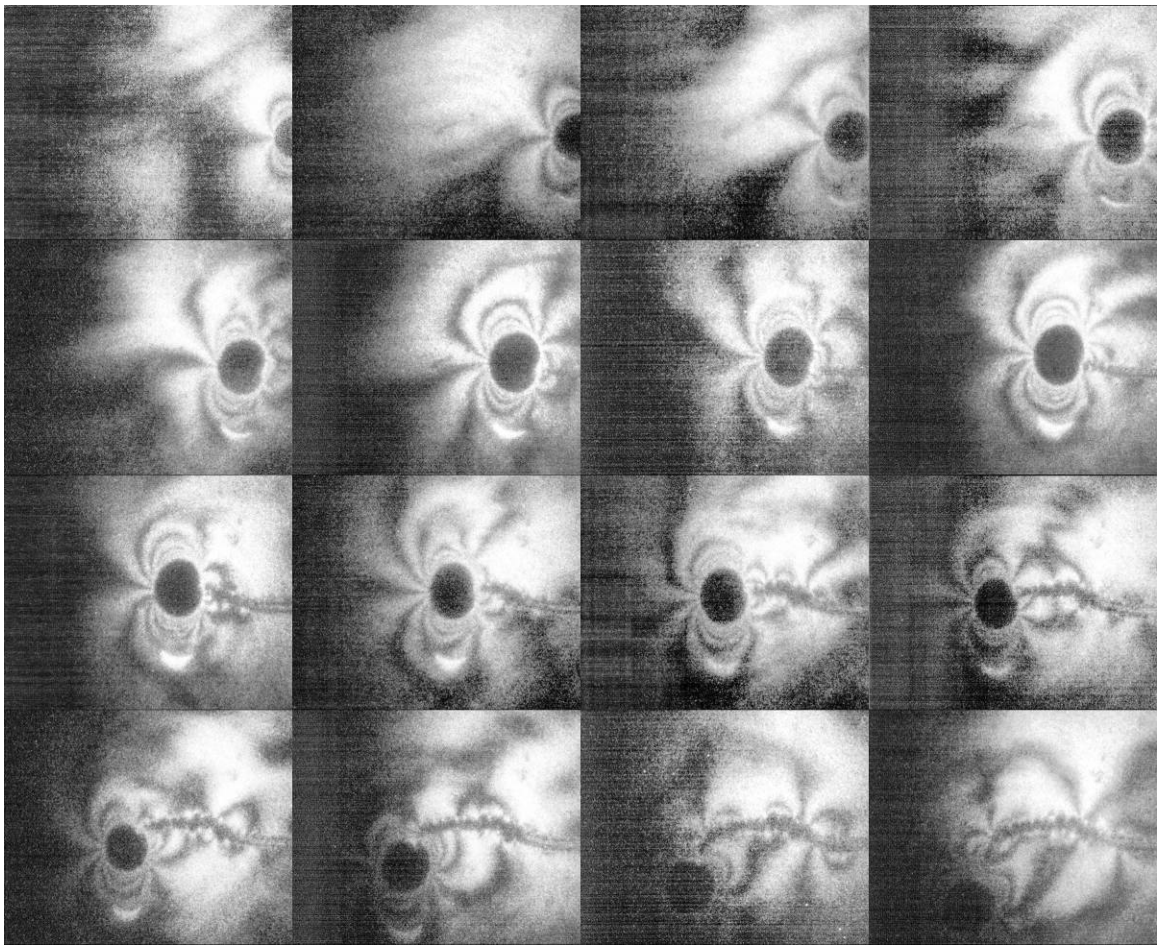

Figure C-24. Shot 177 – PMMA.

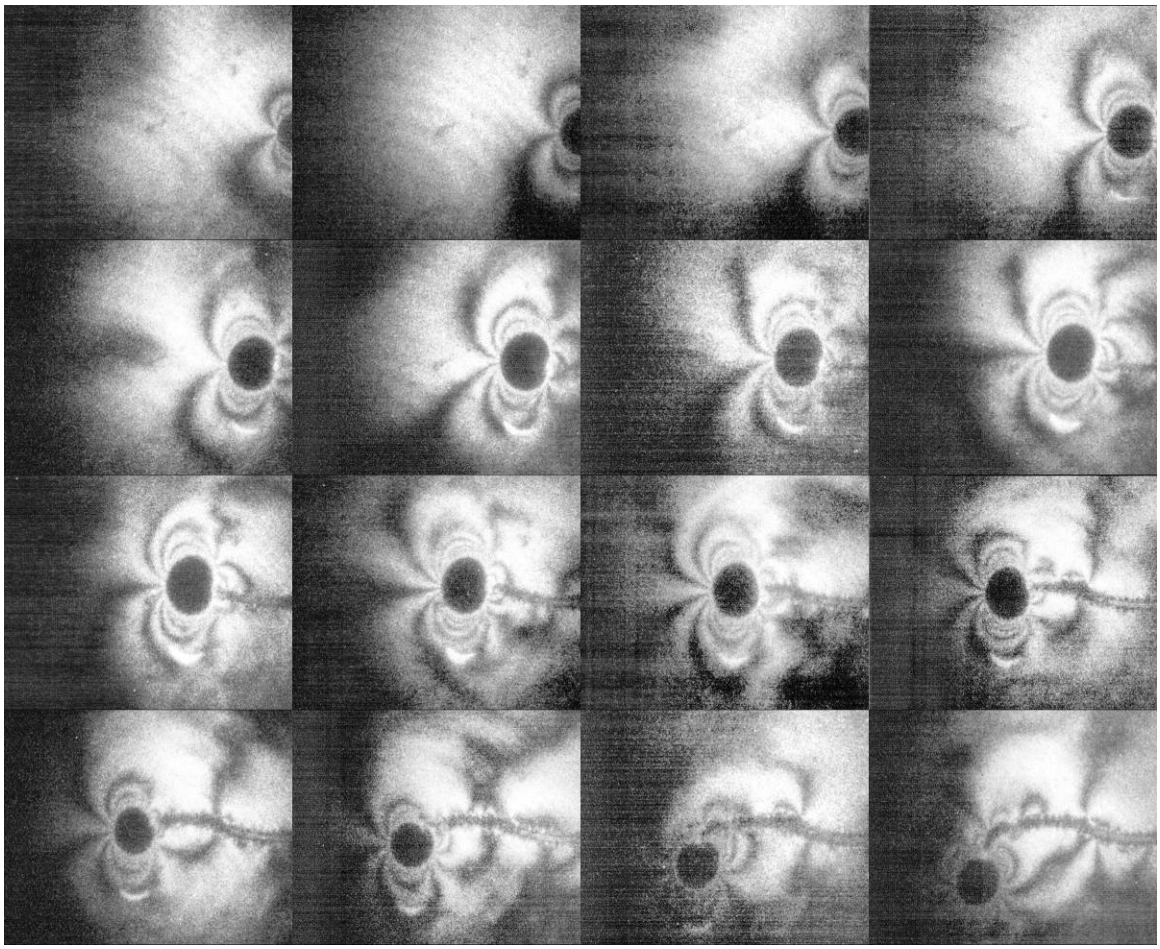

Figure C-25. Shot 178 – PMMA.

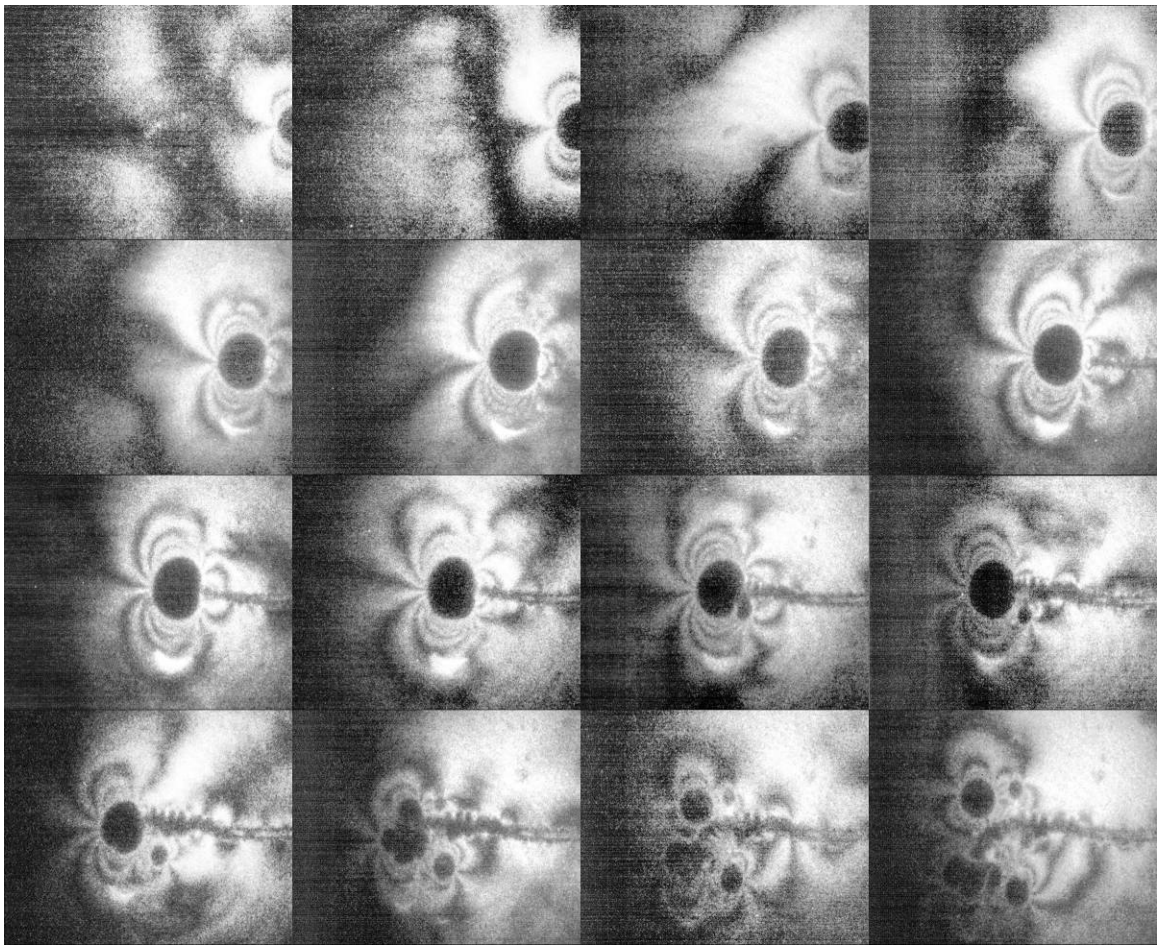

Figure C-26. Shot 179 – PMMA.

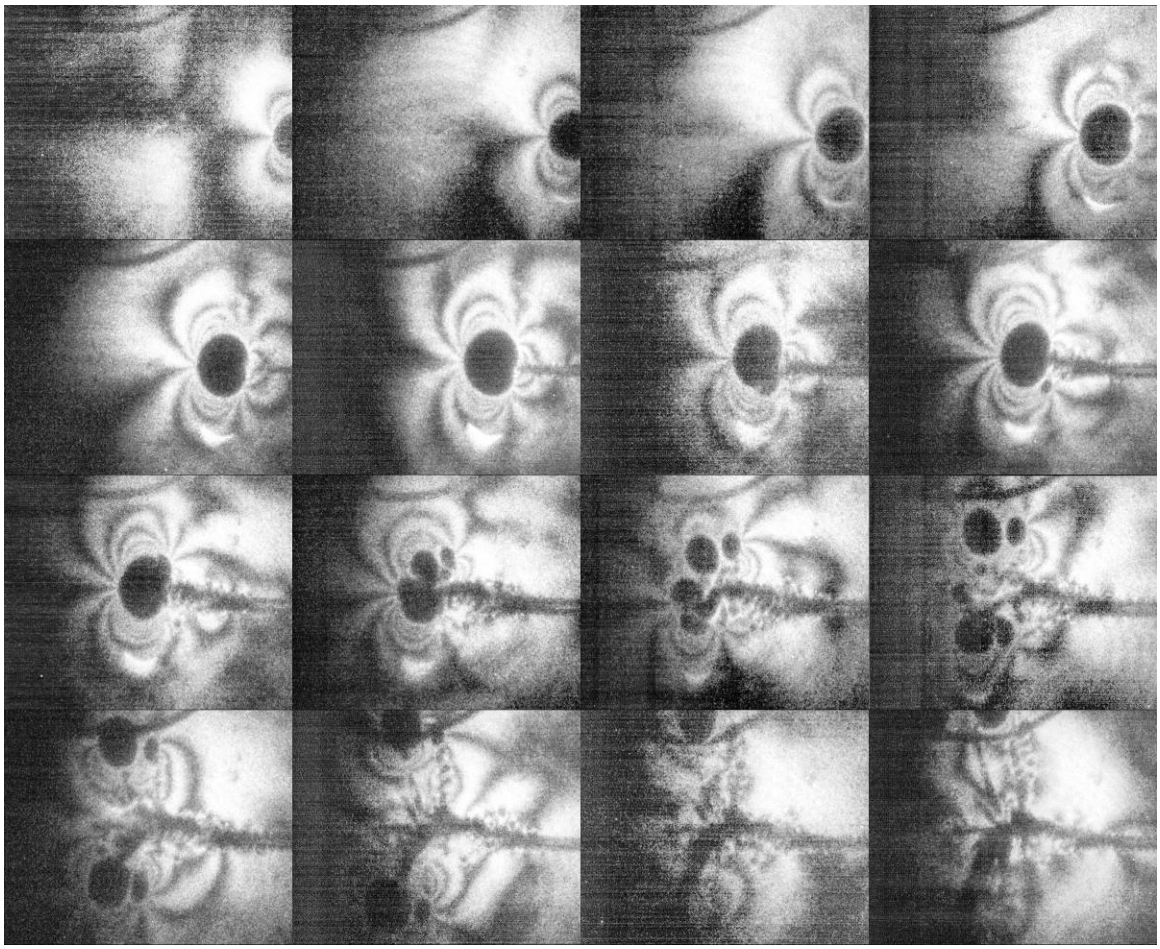

Figure C-27. Shot 180 – PMMA.

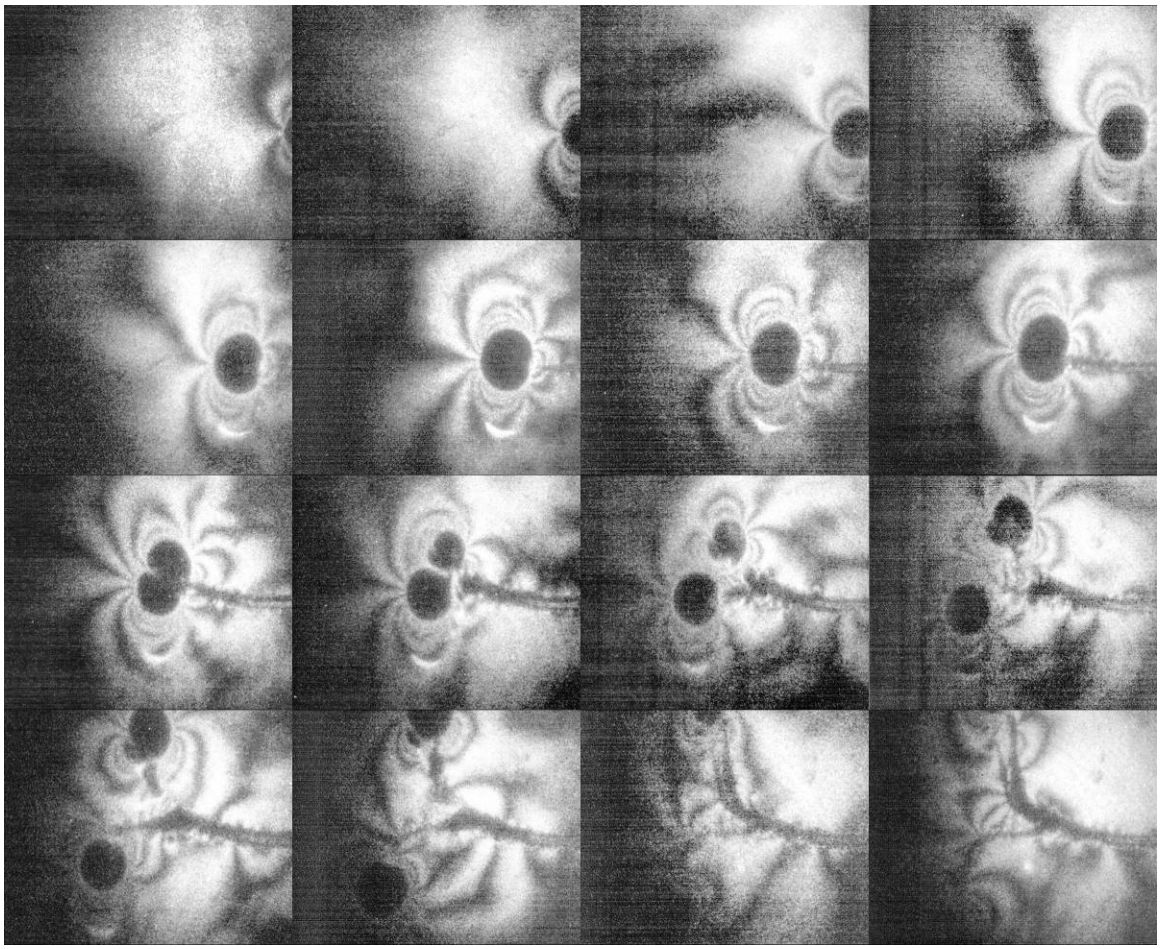

Figure C-28. Shot 181 – PMMA.

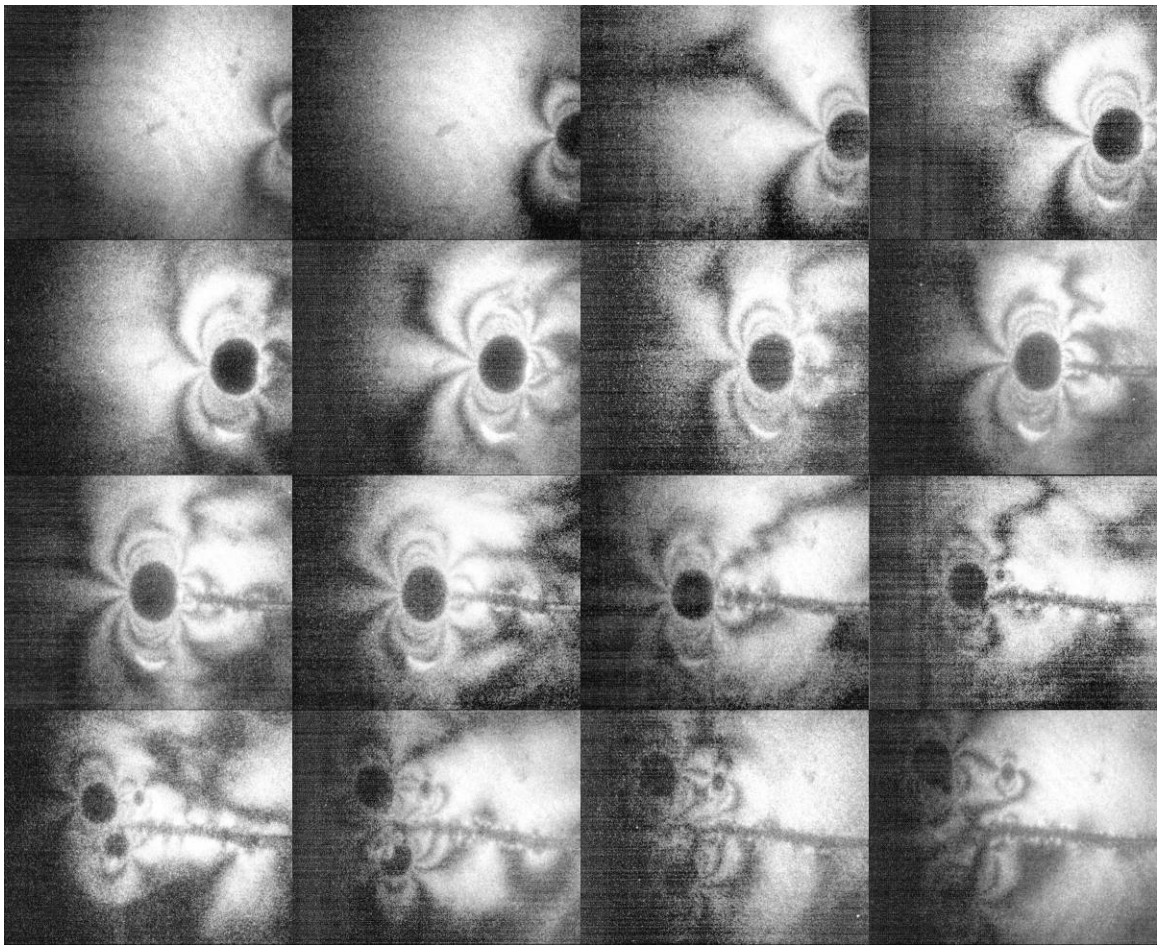

Figure C-29. Shot 182 – PMMA.

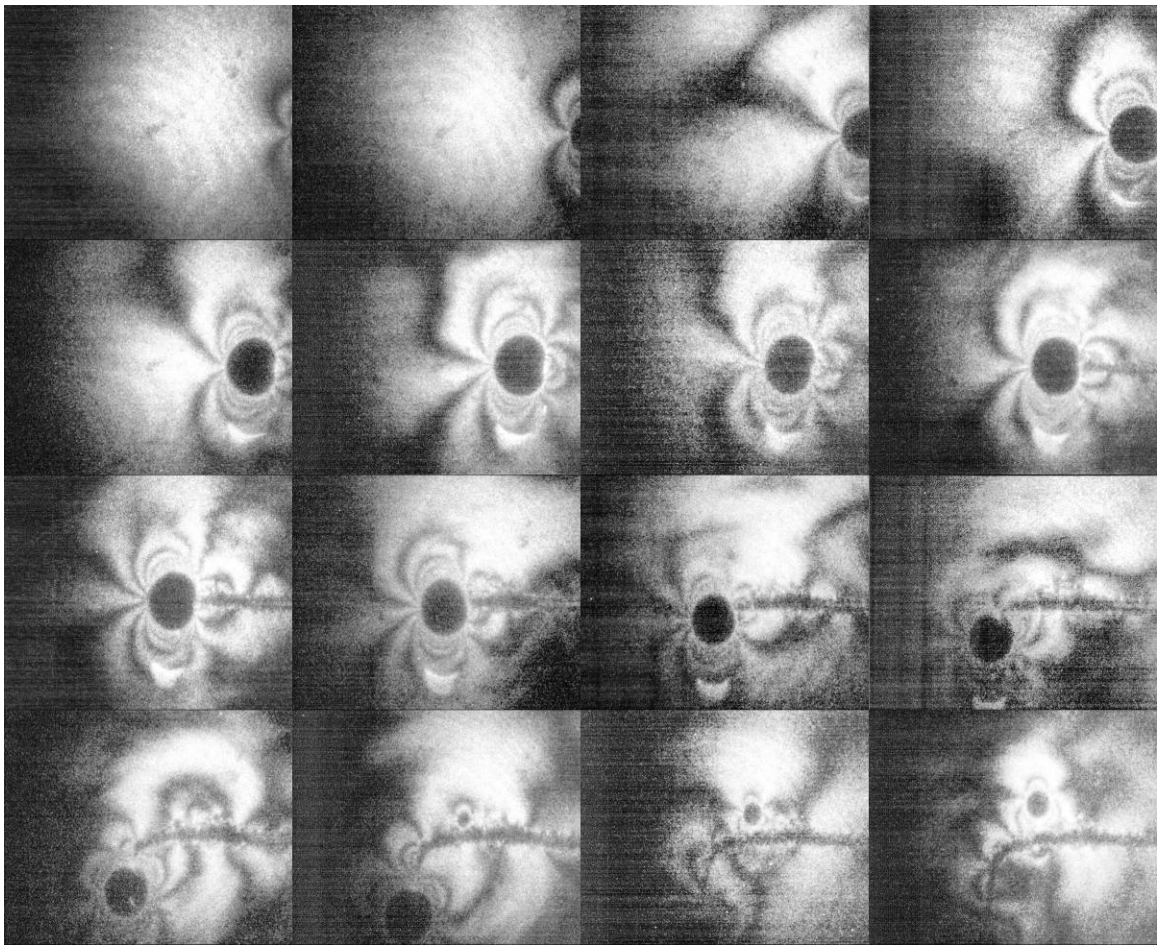

Figure C-30. Shot 183 – PMMA.

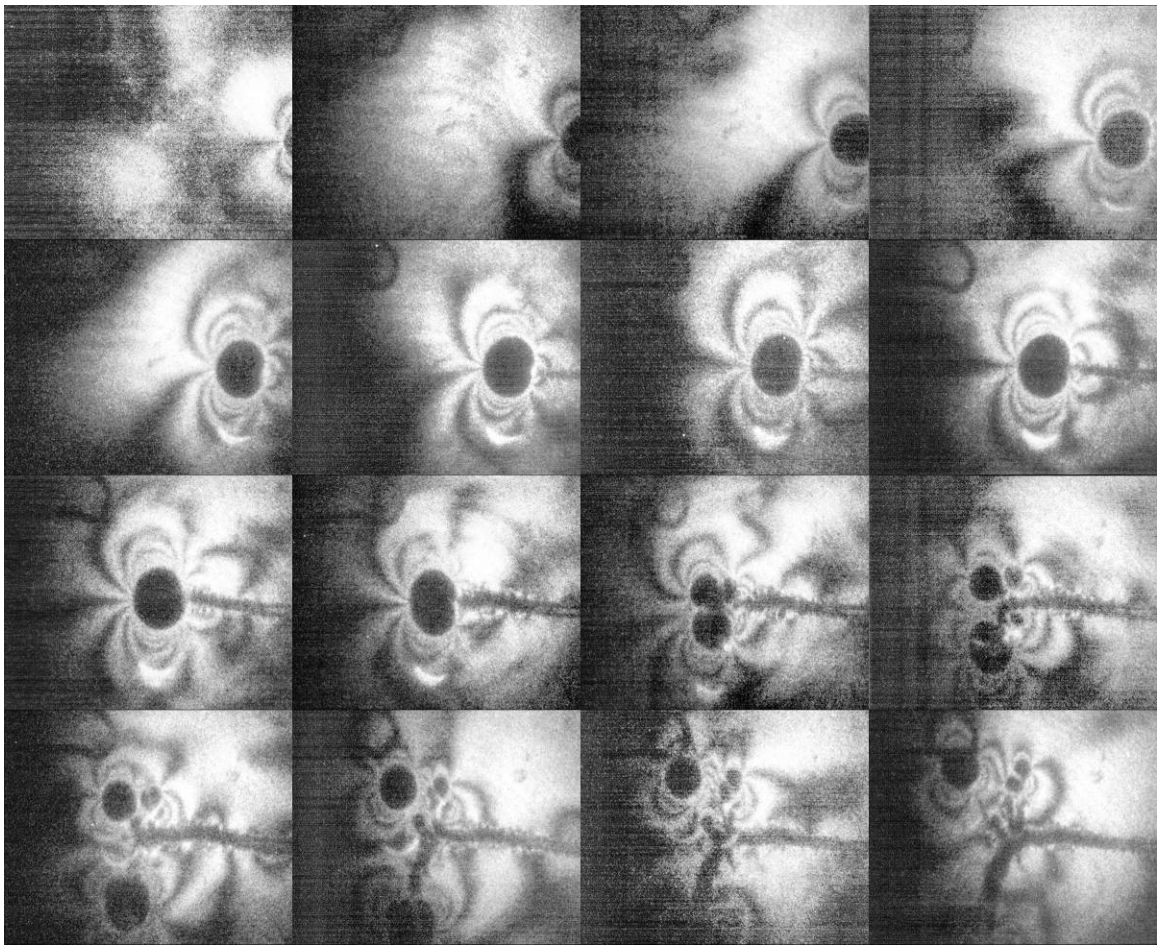

Figure C-31. Shot 184 – PMMA.

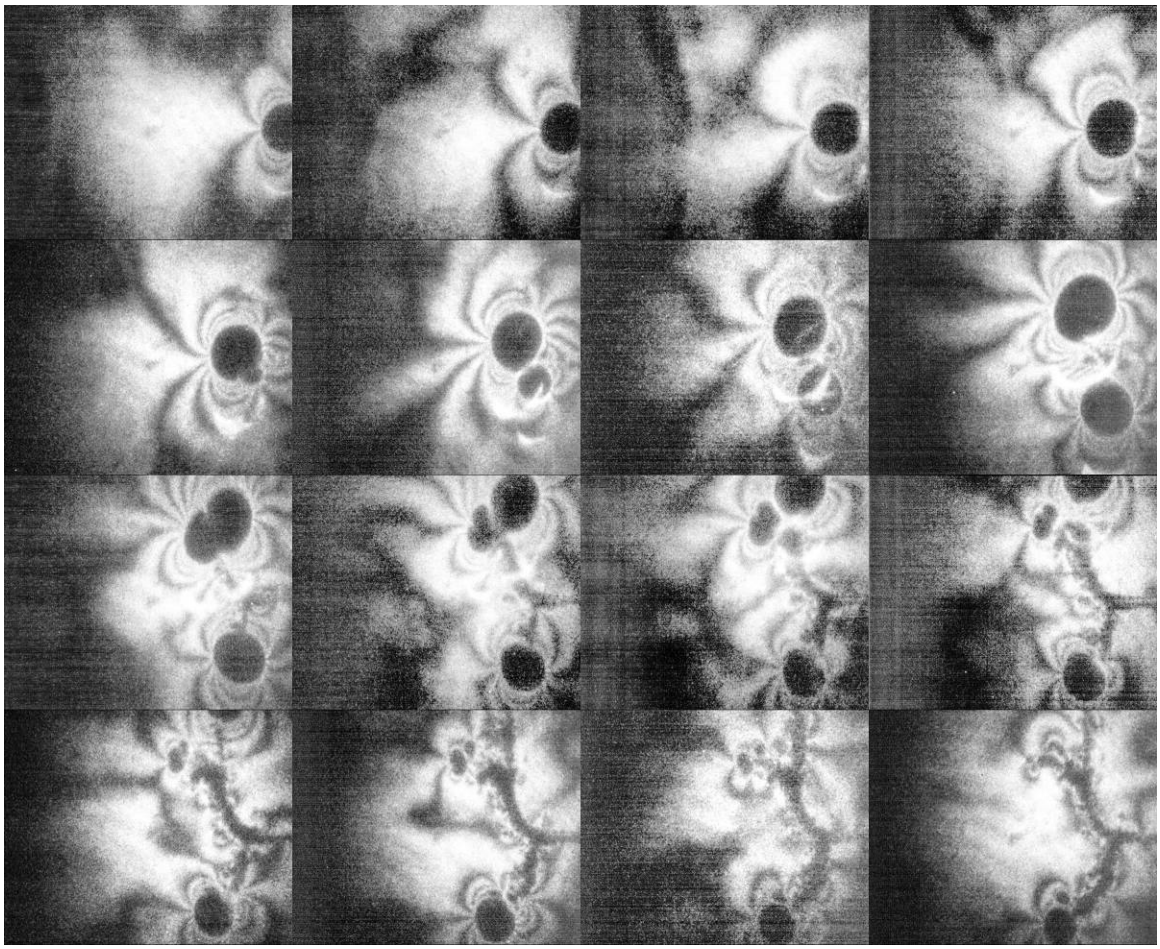

Figure C-32. Shot 185 – PMMA.

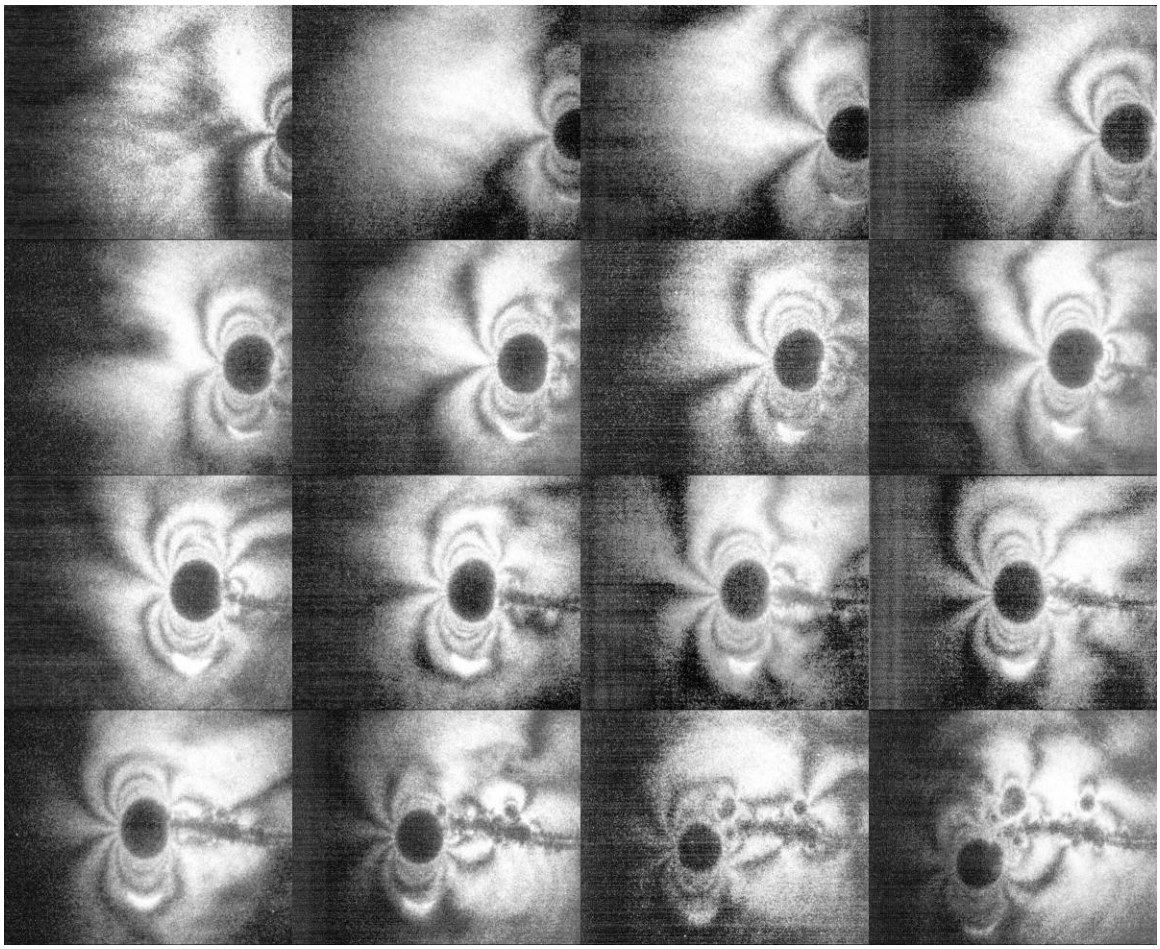

Figure C-33. Shot 186 – PMMA.

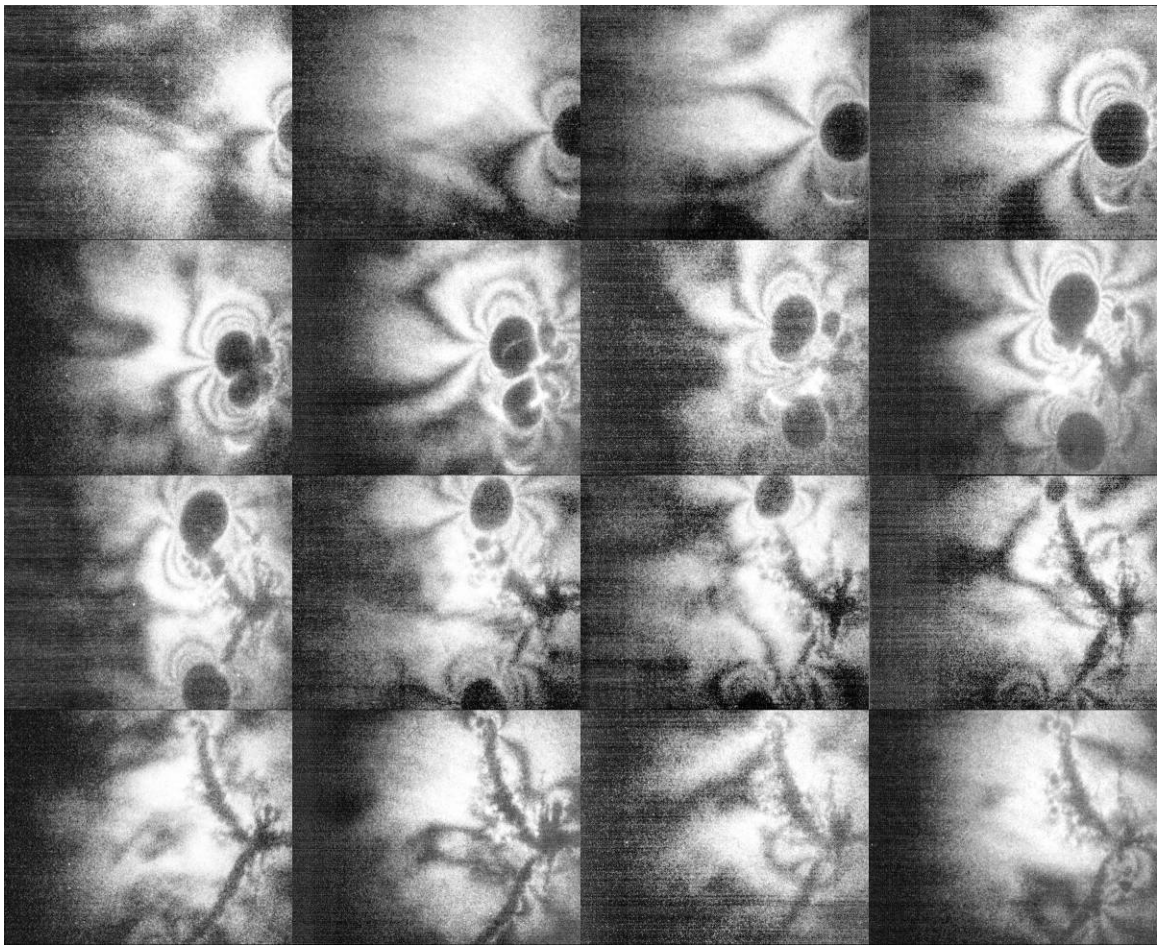

Figure C-34. Shot 187 – PMMA.

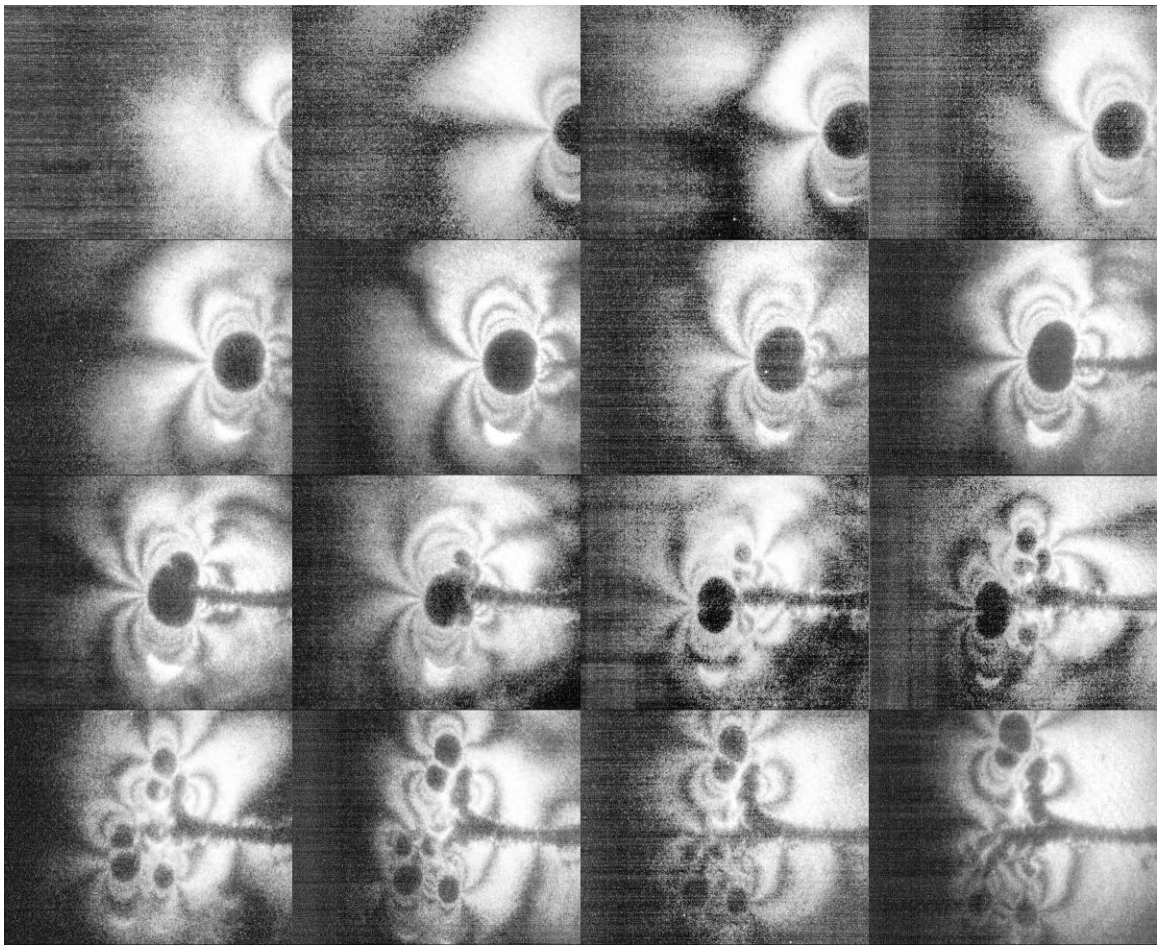

Figure C-35. Shot 188 – PMMA.

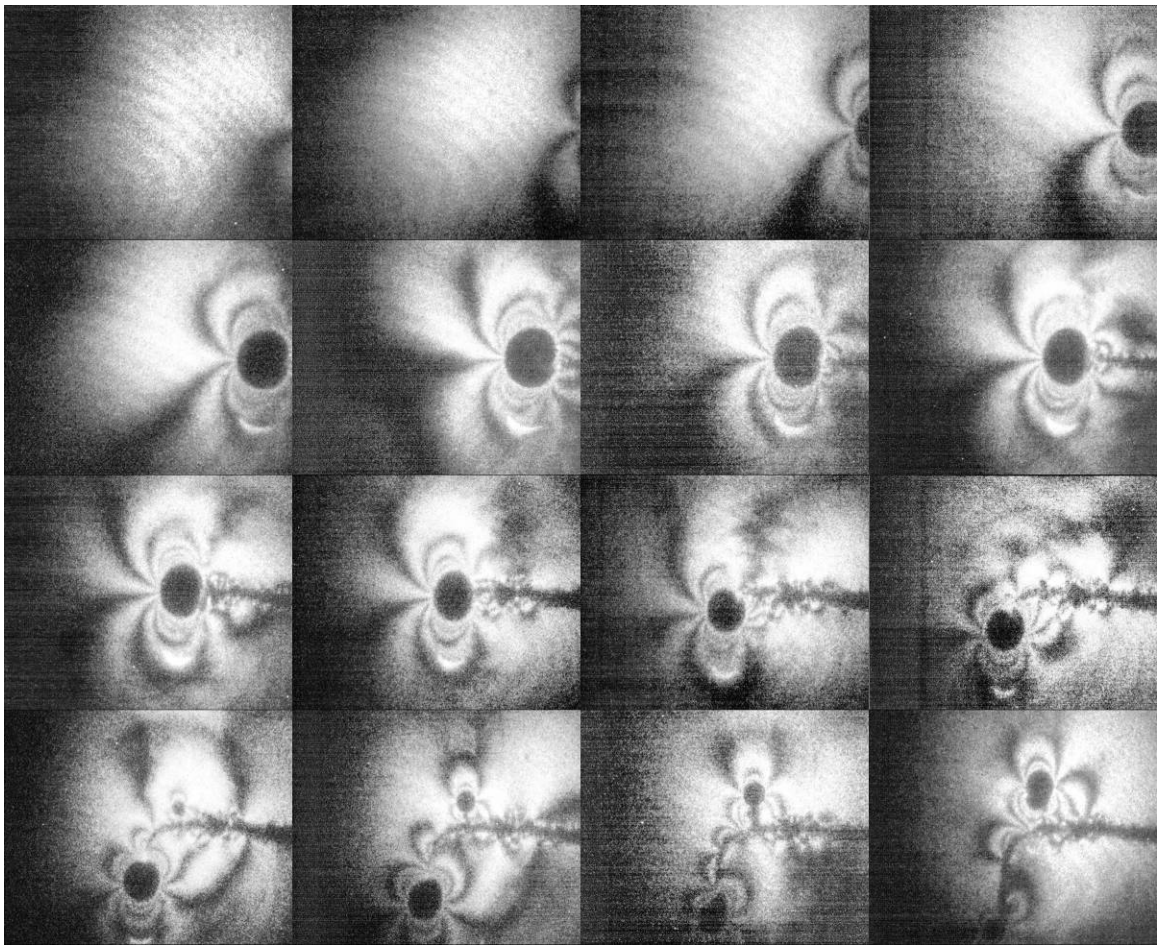

Figure C-36. Shot 189 – PMMA.

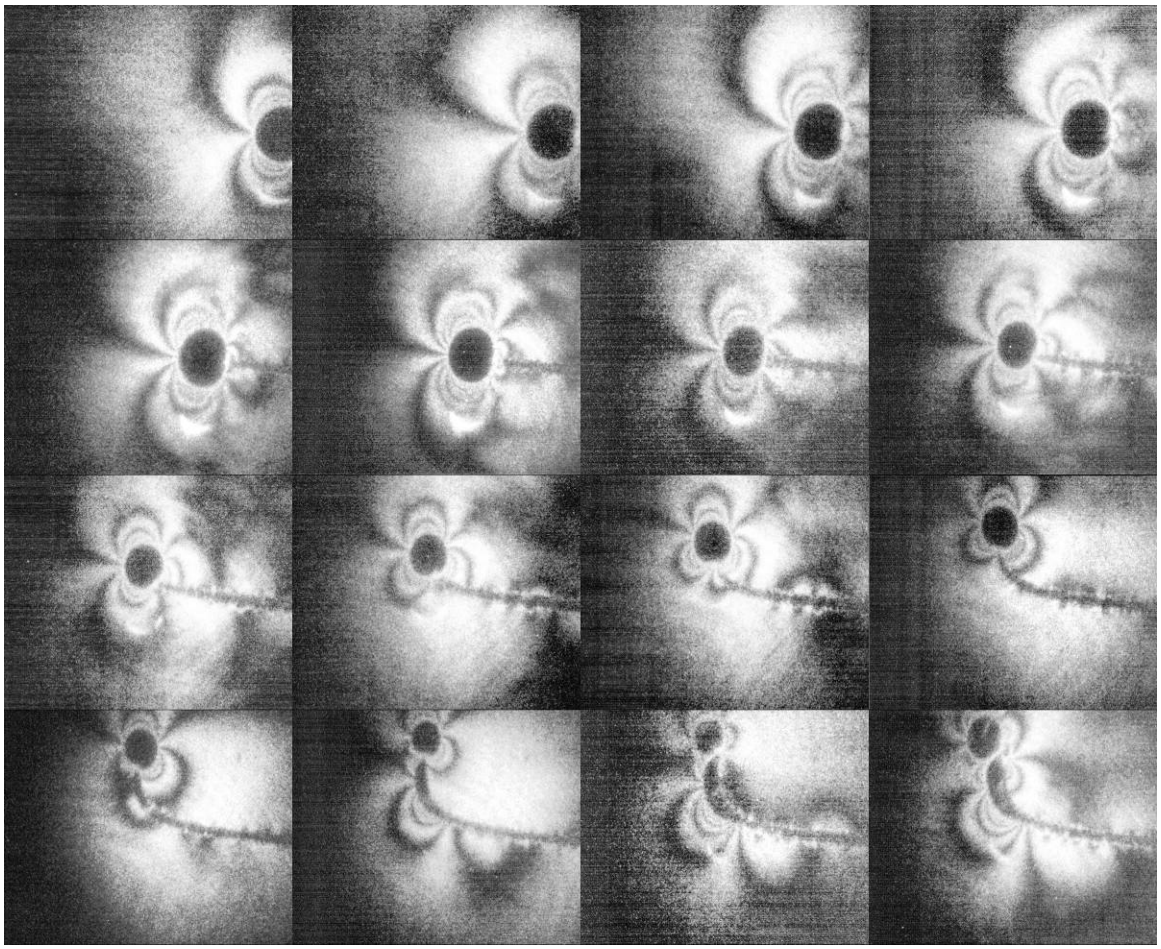

Figure C-37. Shot 190 – PMMA.

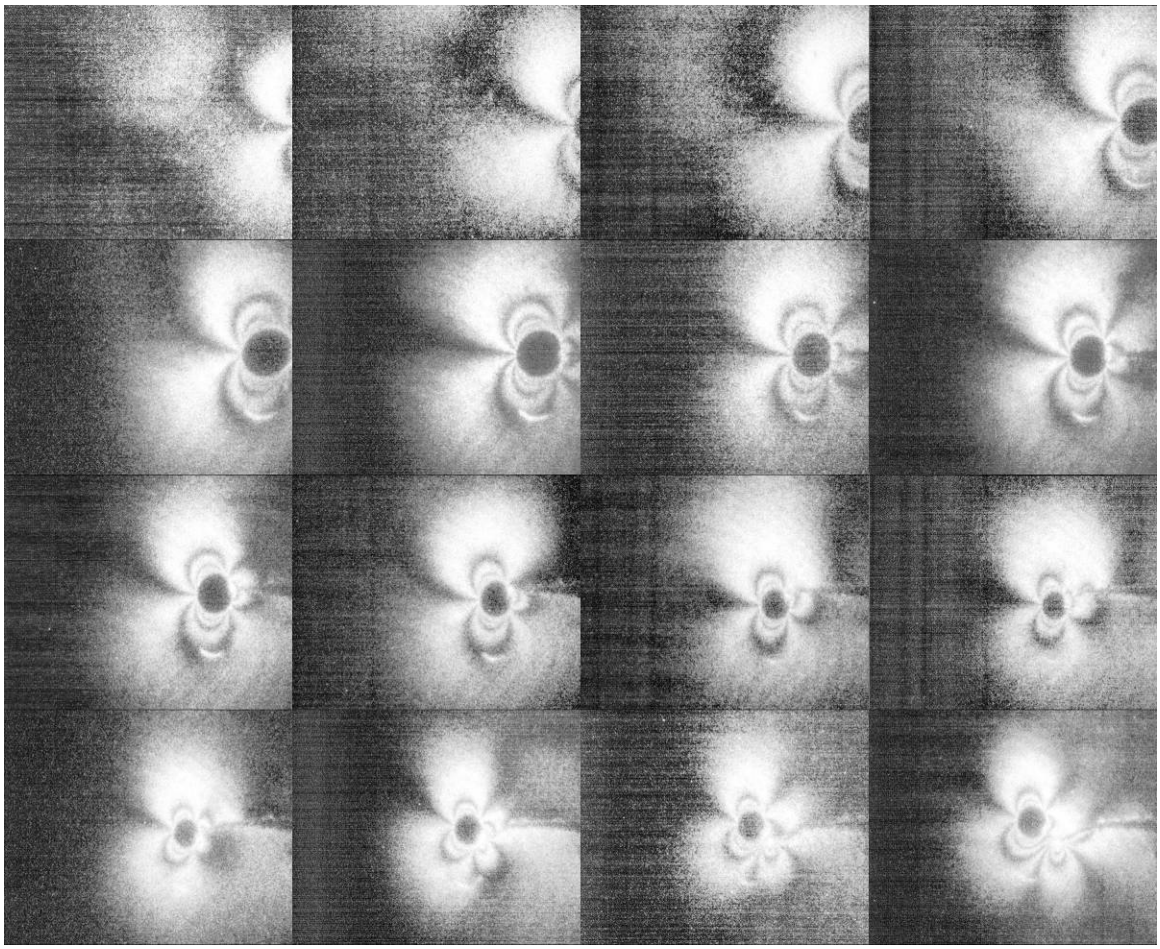

Figure C-38. Shot 191 – PMMA.

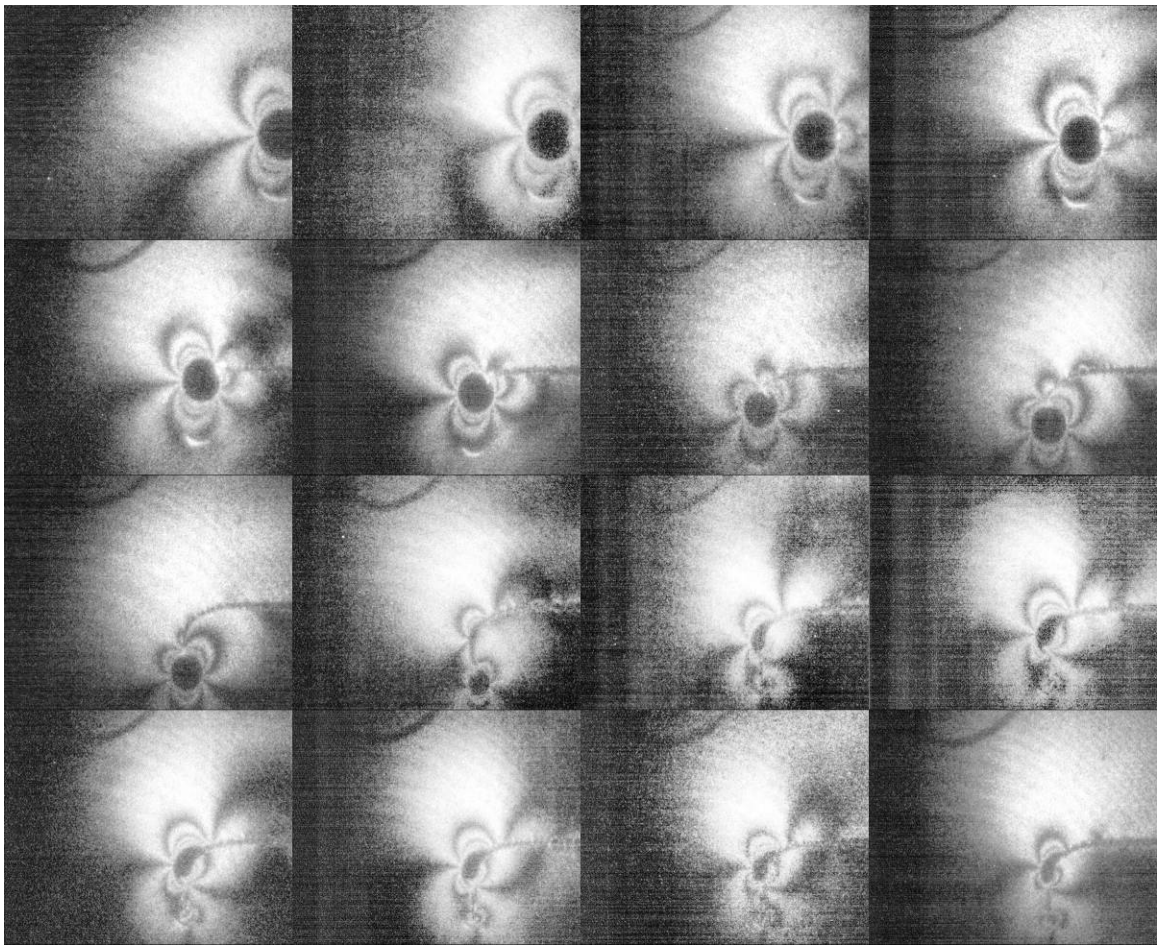

Figure C-39. Shot 192 – PMMA.

NO. OF
COPIES ORGANIZATION

1 (PDF only) DEFENSE TECHNICAL INFORMATION CTR
DTIC OCA
8725 JOHN J KINGMAN RD
STE 0944
FORT BELVOIR VA 22060-6218

1 DIRECTOR
US ARMY RESEARCH LAB
IMNE ALC HRR
2800 POWDER MILL RD
ADELPHI MD 20783-1197

1 DIRECTOR
US ARMY RESEARCH LAB
RDRL CIM L
2800 POWDER MILL RD
ADELPHI MD 20783-1197

1 DIRECTOR
US ARMY RESEARCH LAB
RDRL CIM P
2800 POWDER MILL RD
ADELPHI MD 20783-1197

ABERDEEN PROVING GROUND

1 DIR USARL
RDRL CIM G (BLDG 4600)

NO. OF
COPIES ORGANIZATION

ABERDEEN PROVING GROUND

17 DIR USARL
RDRL WMM A
T WEERASOORIYA
RDRL WMP B
C HOPPEL
T BJERKE
S BILYK
D CASEM
W EDMANSON
R KRAFT
B LOVE (10 CPS)